CRANFIELD UNIVERSITY

XIAOJIAN HUANG

CFD MODELLING OF VAWT WAKE EFFECTS

School of Water, Energy and Environment
MPhil in Energy

MPhil

Academic Year: 2016

Supervisor: Professor Feargal Brennan
December 2016

CRANFIELD UNIVERSITY

School of Water, Energy and Environment
MPhil in Energy

MPhil

Academic Year 2016

Xiaojian Huang

CFD Modelling of VAWT Wake Effects

Supervisor: Professor Feargal Brennan
December 2016

This thesis is submitted in partial fulfilment of the requirements for the degree of MPhil

ABSTRACT

Wake effects are important to wind turbine design and wind farm design, because they will affect the aerodynamic performance and structural loads of wind turbine operating in a wind farm.

Wake effects were investigated extensively for horizontal axis wind turbine(HAWT) in the past, but there has been very limited work done for the vertical axis wind turbine(VAWT), whose wake effects are unique because the blades will go through their own wake region during the operation. The presented thesis aims to bridge this knowledge gap by modelling the VAWT wake effects using CFD.

As for the general wind turbine wake effects study, four key aspects can be identified: wake models, aerodynamics, structural dynamics, and structural integrity. Relevant literature is reviewed in the thesis, and a comprehensive framework of studying the VAWT wake effects is proposed. The framework covers all the four key aspects of the wind turbine wake effects study, and two of them will be addressed in the presented thesis, wake models and wake aerodynamics.

CFD modelling in the thesis is based on RANS method. The near wake modelling focuses on the aerodynamics prediction and the far wake modelling focuses on the wake structure prediction.

As for the near wake study, wake effects of a circular cylinder at Re=140000 is studied and validated. the aerodynamic performance of NACA0015 airfoil at various angle of attack at Re=2000000 is modelled using different turbulence models, dynamic stall effects of the airfoil at three different regimes are investigated. They form the basis of analysing the aerodynamic performance of VAWT rotor. A 17m 2-bladed VAWT designed based on such geometries (circular cylinder and NACA0015 airfoil) is modelled thereafter, simulated aerodynamic performance under different tip-speed ratios are compared with experiment data.

As for the far wake study, both rotor simplification using porous disk and full rotor simulation are presented. A persistent symmetric wake region is observed from

the porous disk modelling while the full rotor modelling predicts an asymmetric wake region. The wake interaction is then studied in a two turbine VAWT array, the influence of wake effects on the performance of VAWT at 3 diameters downstream is investigated. Overlapping of wake region is analysed.

Keywords:

Wake effects, VAWT, CFD, RANS, Aerodynamics

Dedicated to my mother

"It was the best of times, it was the worst of times, it was the age of wisdom, it was the age of foolishness, it was the epoch of belief, it was the epoch of incredulity, it was the season of light, it was the season of darkness, it was the spring of hope, it was the winter of despair, we had everything before us, we had nothing before us, we were all going direct to heaven, we were all going direct the other way – in short, the period was so far like the present period, that some of its noisiest authorities insisted on its being received, for good or for evil, in the superlative degree of comparison only."

----From *A Tale of Two Cities* by Charles Dickens

"博學之，審問之，慎思之，明辨之，篤行之"

——《中庸》

"*To this attainment there are requisite the extensive study of it, accurate inquiry about it, careful reflection on it, the clear discrimination of it, and the earnest practice of it.*"

——From *the Doctrine of the Mean* by Confucius

ACKNOWLEDGEMENTS

The thesis would not be possible without many individuals and institutions.

First and foremost, I would like to express my deepest gratitude to Professor Feargal Brennan for his enormous patience and wisdom in supervising me. Communication with him has helped me realise my limitations and pushed me to reach my full potentials.

I would also like to thank Dr Andrew Shires for his advice in my CFD simulation works at early stage of my study. I learned a lot from the discussion with him.

I am indebted to Professor Liu Yongqian and Professor Tian De who brought me to wind energy since 2006, and gave me a lot encouragement since the commence of the project.

I want to express my sincere gratitude to all my colleagues: Payam, Wilson, Bello, Michael, Grammar, Adamu, Dawid for creating an active and inspiring study environment, and especially to Shiwei and Jing, who help me a lot throughout all these years and provide me enormous mental support.

I would like to thank Athanasius, Maurizio, and other staff at Cranfield, especially Sam and Nicola for their timely assistance

I am grateful to China Scholarship Council (CSC) and North China Electric Power University(NCEPU), my sponsor and former university, for their financial support and administration throughout my study in UK.

Finally, I would like to thank my family, for their warmest love and firm support in my great endeavour.

TABLE OF CONTENTS

ABSTRACT i
ACKNOWLEDGEMENTS iv
LIST OF FIGURES vii
LIST OF TABLES ix
LIST OF EQUATIONS x
LIST OF ABBREVIATIONS xii
NOMENCLATURE xiii
1 INTRODUCTION 1
1.1 Research Background 1
1.2 Aim and Objectives 3
1.3 Thesis Outline 3
2 LITERATURE REVIEW 5
2.1 Wind Energy Technology 5
2.2 Wake Effects Research: State-of-the-Art 7
2.2.1 Overview 7
2.2.2 Experiments 10
2.2.3 Modelling 12
2.3 Aerodynamic Analysis Methods 16
2.3.1 Overview 16
2.3.2 BEM method 16
2.3.3 Vortex method 18
2.3.4 CFD method 20
2.4 CFD on STAR-CCM+ 22
2.4.1 Overview 22
2.4.2 Governing equations 23
2.4.3 Mesh generation 24
2.4.4 Turbulence models 25
2.5 Summary 29
3 NEAR WAKE MODELLING 31
3.1 Introduction 31
3.2 Cylinder Wake Modelling 31
3.2.1 Overview 31
3.2.2 Simulation setup 36
3.2.3 Results and discussion: 38
3.3 Airfoil Modelling 43
3.3.1 Static stall 43
3.3.2 Dynamic stall 47
3.4 Rotating VAWT Modelling 52
3.4.1 Overview 52
3.4.2 Simulation setup 54

3.4.3 Results and discussion 57
3.5 Summary 59
4 FAR WAKE MODELLING 61
4.1 Introduction 61
4.2 Porous Disk Modelling 61
4.2.1 Overview 61
4.2.2 Simulation setup 61
4.2.3 Results and discussion 62
4.3 2D Full Rotor Modelling of Single VAWT 67
4.3.1 Overview 67
4.3.2 Simulation setup 67
4.3.3 Results and discussion 67
4.4 2D Full Rotor Modelling of VAWT Array 69
4.4.1 Overview 69
4.4.2 Simulation setup 69
4.4.3 Results and discussion 70
4.5 Summary 75
5 CONCLUSION 77
5.1 Summary and Conclusion 77
5.2 Contribution to Knowledge 78
5.3 Limitation and Future Work 78

LIST OF FIGURES

Figure 1-1 Conventional wind farm of horizontal axis wind turbine..... 1
Figure 1-2 Study framework of wake effects 2
Figure 2-1 Schematic division of wake regions 8
Figure 2-2 Role of CFD 21
Figure 2-3 Different types of CFD Methods..... 22
Figure 3-1 GALCIT Wind Tunnel..... 35
Figure 3-2 2D mesh for modelling cylinder wake..... 36
Figure 3-3 Wall Y+ value check in 2D 37
Figure 3-4 Cylinder surface pressure prediction..... 40
Figure 3-5 Line probes for wake profile 40
Figure 3-6 Cylinder wake velocity profile prediction 41
Figure 3-7 Line probes for centreline velocity..... 42
Figure 3-8 Centreline velocity behind the cylinder..... 42
Figure 3-9 Centreline velocity comparison 42
Figure 3-10 NACA00XX airfoil..... 43
Figure 3-11 2D mesh of NACA 0015 Airfoil..... 44
Figure 3-12 Lift coefficient of NACA0015 airfoil of three models 46
Figure 3-13 Local angle of attack at different tip speed ratios 47
Figure 3-14 Lift coefficient prediction of NACA0015 airfoil at $\alpha=4°+4°*sin\omega t$.. 50
Figure 3-15 Lift coefficient prediction of NACA0015 airfoil at $\alpha=11°+4°*sin\omega t$ 50
Figure 3-16 Lift coefficient prediction of NACA0015 airfoil at $\alpha=17°+5°*sin\omega t$ 51
Figure 3-17 Velocity contour of NACA0015 at deep stall 52
Figure 3-18 Configuration of SNL 17m VAWT..... 53
Figure 3-19 velocity contour of SNL-17m VAWT TSR=4.6..... 56
Figure 3-20 Velocity contour of SNL-17m VAWT TSR=2.33..... 56
Figure 3-21 Normal and tangential force coefficient of VAWT..... 58
Figure 4-1 Velocity contour of flow around porous disk..... 63
Figure 4-2 Turbulence length scale impact 64

Figure 4-3 Turbulence intensity impact 65
Figure 4-4 Solver constants change 66
Figure 4-5 Schematic of 2D far wake modelling of SNL-17m VAWT 67
Figure 4-6 Far wake modelling of single VAWT in 2D(λ=2.33) 68
Figure 4-7 Far wake modelling of single VAWT in 2D(λ=4.6) 68
Figure 4-8 Far wake modelling configuration of SNL 17m VAWT array 69
Figure 4-9 Wake velocity contour of VAWT array 72
Figure 4-10 Force coefficient of upstream VAWT 73
Figure 4-11 Force coefficient of downstream VAWT 73
Figure 4-12 Force coefficient of two VAWTs (k-ε) 74
Figure 4-13 Force coefficient of two VAWTs (k-ω) 74
Figure 4-14 Force coefficient of two VAWTs (S-A) 75

LIST OF TABLES

Table 2-1 A List of code for wake effects modelling 15
Table 2-2 List of aerodynamic analysis tools 20
Table 3-1 Configuration of GALCIT Experiment 35
Table 3-2 2D Mesh sensitivity analysis 37
Table 3-3 Cylinder vorticity contour of five models 39
Table 3-4 Lift coefficient of NACA 0015 airfoil at Re=2000000 46
Table 3-5 Configuration of dynamic stall cases 48
Table 3-6 Parameters used for defining motion in STAR-CCM+ 48
Table 3-7 Key Parameter of 2D simulation 53
Table 4-1 Test cases for the porous disk 62

LIST OF EQUATIONS

(2-1)..... 9
(2-2)..... 9
(2-3)..... 9
(2-4)..... 9
(2-5)..... 9
(2-6)..... 9
(2-7)..... 9
(2-8)..... 9
(2-9)..... 10
(2-10)..... 23
(2-11)..... 23
(2-12)..... 23
(2-13)..... 24
(2-14)..... 24
(2-15)..... 24
(2-16)..... 24
(2-17)..... 26
(2-18)..... 26
(2-19)..... 26
(2-20)..... 26
(2-21)..... 26
(2-22)..... 26
(2-23)..... 26
(2-24)..... 26
(2-25)..... 26
(2-26)..... 26
(2-27)..... 26
(2-28)..... 27

(2-29)..... 27
(2-30)..... 27
(2-31)..... 27
(2-32)..... 27
(2-33)..... 27
(2-34)..... 27
(2-35)..... 27
(2-36)..... 28
(2-37)..... 28
(2-38)..... 28
(2-39)..... 28
(2-40)..... 28
(2-41)..... 28
(2-42)..... 29
(2-43)..... 29
(2-44)..... 29
(2-45)..... 29

LIST OF ABBREVIATIONS

ABL	Atmospheric Boundary Layer
ACD	Actuator Disc
ACL	Actuator Line
AEP	Annual Energy Production
BEM	Blade Element Momentum
CFD	Computational Fluid Dynamics
DNS	Direct Numerical Simulation
FEA	Finite Element Analysis
FEM	Finite Element Method
HAWT	Horizontal Axis Wind Turbine
IT	Information Technology
LES	Large Eddy Simulation
PSD	Power Spectral Density
RANS	Reynolds Averaged Navier-Stokes
RMS	Root Mean Square
SST	Shear Stress Transport
VAWT	Vertical Axis Wind Turbine
VTM	Vorticity Transport Method

NOMENCLATURE

C_T	Thrust coefficient
C_p	Power coefficient
I_{add}	Wake added turbulence
I_{eff}	Equivalent wake turbulence
Re_c	Reynolds number based on chord
S_{v-m}	Von Mises stress
r_t	Leading edge radios
y^+	Dimensionless wall distance
z_0	Roughness length
$\mathcal{G}(f)_j$	PSD of the stress
h	Thickness of the atmospheric boundary layer
B	Solidity
D	Rotor diameter
E	Young's modules
H	Rotor height
I	Turbulence intensity
L	Length Scale
M	Mass
N	Number of blades
P	Power
P	Pressure
Re	Reynolds number
S	Swept area
S	Stress
St	Strouhal Number
V	Wind speed
a	Induction factor
c	Blade chord length
f	Frequency
t	Time
z	Distance from the ground

α	Angle of attack
δ	Boundary layer thickness
ε	Strain
θ	Azimuthal angle
λ	Tip speed ratio
μ	Dynamic viscosity
τ	Shear stress

1 INTRODUCTION

1.1 Research Background

Wind energy is clean and renewable energy with great potential. Wind turbine technology has developed quickly in the past decades. According to statistics of GWEC, global cumulative installed wind capacity has reached 369.5 GW by 2014. (GWEC, 2015)

To exploit the rich wind resource offshore, more wind farms are building offshore in recent years, and there is a resurgence of interests for VAWT in offshore applications. VAWT possesses a number of merits (Islam et al., 2008): A main advantage of VAWT is that no yaw mechanisms are required, thus simplifying the design configurations significantly; Blades of straight-bladed VAWT may be of uniform section and untwisted, making them relatively easy to fabricate or extrude; Furthermore, almost all of the components of VAWT requiring maintenance are located at the ground level, facilitating the maintenance work appreciably.

An early investigation of Goldenberg (Goldenberg and Fekete, 1983) found out that vertical axis wind turbine could be placed closer because the enhanced mixing of flow. A more recently investigation by Whittlesey (Whittlesey et al., 2010, Dabiri, 2011) investigated the fish schooling effects of small VAWT clusters, results shows that by counter rotating the rotor, the wind farm efficiency can be higher than existing wind farm. Therefore, it is conceivable that a cost-effective wind farm consisting of VAWTs could be built in the future.

Figure 1-1 Conventional wind farm of horizontal axis wind turbine

The deployment of VAWT in wind farm faces challenges from wake effects. Wake is a flow region behind the rotor where velocity is reduced and turbulence intensity changes. Wake effects are one interesting issue to tackle for wind turbine operating in wind farm because wake does not only influence the power performance of the downwind turbines, but also gives rise to extra structural loads and affects the fatigue life of them.(Crespo et al., 1999) In particular for VAWT, the aerodynamic interaction occurs between the blades and wakes from itself and upstream turbine poses significant engineering challenge in the operation. Comprehensive knowledge of VAWT wake effects is needed for the prediction of wind farm annual energy production(AEP) and the maintenance cost, to reduce the investment risks and make wind energy more competitive.

Wake effects have been studied extensively for HAWT, however they are not fully understood for VAWT. The presented thesis aims to improve the understanding of VAWT wake effects.

There are four key elements of wake effects study: 1) wake model study, 2) wake aerodynamics study, 3) wake structural dynamics study, 4) wake structural integrity study. A framework for study wake effects is shown in Figure 1-2. Wake model study is dedicated to predicting the far wake properties such as velocity deficit and turbulence structure behind a rotor. Wake aerodynamics study concerns the aerodynamic forces exerted on a structure, and the prediction of aerodynamic performance/loading for wind turbine at different operation conditions. The task of wake structural dynamics is to predict the wind turbine response to wind loading when it operates in wake. Finally, wake structural integrity study is to ensure wind turbines safety over lifetime in the presence of wake loads.

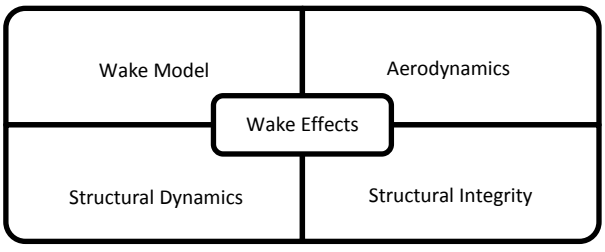

Figure 1-2 Study framework of wake effects

1.2 Aim and Objectives

Instead of covering all four elements, the presented thesis will only focus on the wake model study and the aerodynamics study of VAWT. It aims to determine the aerodynamic performance and wake velocity distribution of VAWT through CFD modelling. This will also lay the foundation for studying other elements in the wake effects study framework as shown in Figure1-2.

It is generally accepted that wake region can be further divided into near wake region and far wake region. Near wake locates right behind the rotor and directly affect the rotor performance, while far wake is a region which ambient turbulence play a more significant role. The primary focus of near wake modelling is the aerodynamic performance of wind turbine and the vortical structure close to the rotor, whereas the primary focus of far wake modelling is to capture the velocity deficit and turbulence properties.

The objectives of the thesis can be summarized as follows:

1) Modelling VAWT aerodynamics and associated near wake phenomenon, and determine the aerodynamic performance of VAWT.

2) Modelling VAWT far wake and wake interaction, and determine the wake velocity distribution.

The two objectives are interconnected because the near wake and far wake will interact with each other. On one hand, the far wake flow behaviour can affect the aerodynamic performance of a downstream wind turbine. On the other hand, the near wake phenomenon such dynamic stall and vortex shedding can influence the onset of far wake velocity distribution.

1.3 Thesis Outline

Chapter 1 provides a general description of the research background as well as the aim and objectives of the research.

Chapter 2 is a review of selected literature. Opportunities and challenges faced by the wind technology are reviewed in Section 2.1. Wind turbine wake effects

research is reviewed in Section 2.2, including experiments and modelling effort. Section 2.3 is included to review the various aerodynamic analysis methods used on wind turbines. As CFD simulation is performed throughout the research, the CFD simulation tool, STAR-CCM+, as well as some underlying mathematical models are introduced in Section 2.4. In Section 2.5, a summary is included to highlight major findings of the literature review.

Near wake modelling and far wake modelling are presented in Chapter 3 and Chapter 4 respectively. The near wake modelling focuses mainly on the aerodynamic performance, whereas the far wake modelling focuses mainly on the wake structure prediction.

Section 3.1 is an introduction of the near wake modelling activity. Section 3.2 to Section 3.4 present a selection of simulation work done for modelling VAWT aerodynamics and the associated near wake phenomenon. Both circular cylinder and airfoils are fundamental parts in designing VAWT, detailed simulations of them can be beneficial to understanding the aerodynamics as well as the far wake structure of VAWT. The aerodynamic performance of a 17m 2-bladed VAWT is modelled at various tip-speed ratios. Key findings of the near wake modelling are included in Section 3.5.

Far wake modelling of VAWT is discussed in Chapter 4, different approaches for modelling the far wake are investigated on STAR-CCM+, focusing on the wake velocity structure prediction. Simplified far wake modelling and full rotor far wake modelling is included in Section 4.2 and Section 4.3 respectively. Full rotor far wake modelling of VAWT array is presented in Section 4.4. Key findings of the far wake modelling are summarized in Section 4.5.

Finally conclusions are made in Chapter 5, where contribution to knowledge and limitation of the presented study are also included.

2 LITERATURE REVIEW

2.1 Wind Energy Technology

Wind energy has long been used in history. Wind energy has been used for power generation in late 19th century. But development of wind energy is in the shadow in the prosperity of traditional fossil fuel energy until the 1970s when the oil crisis happened. Out of the concern of energy security, many European countries and the USA starts investing in the research of wind energy.

In the 1990s, as the depletion of traditional fossil fuel, and the increasing awareness of the global warming and climate change, clean and renewable energy demand are increasing. Wind energy has gain some technology edge compared to other renewable energy forms such as biomass, solar, and wave and tidal energy, and become the front-runner in the competition of renewable energy. Since the Kyoto protocol and the introduction of Clean Development Mechanism, wind energy installation has experience a great leap in the last decades, especially in developing countries such as China. The massive scale installation also comes hand in hand with further reduction of energy cost, and stimulate further exploration of technology options, in aim of increasing the production and bringing down the cost of energy.

The uneven solar radiation on earth results in a pressure difference that moves the air and wind is formed.

Meteorologists regard wind as an atmospheric motion, and divide wind into different scales according to time or length. Spatially, the largest scale could be more than 100km, mesoscale could be 10km and microscale could be 100 meters, temporally, scales of wind could be far less than a second or up to many years. These scales are valuable parameter to evaluate the varying wind.

Wind energy generally refers to the kinetic energy of the moving air. The mass flow rate of air over an area can be expressed as a function of density, and area and air velocity. The power output is therefore proportional to air velocity to the third power. From this point of view, the wind energy potential on earth is massive. Wind turbine is a rotating machinery (at least till now) to convert this energy. It is

already known that there exists a theoretical limit for wind turbine. The Betz limit, 0.593, is the maximum efficiency a wind turbine could reach assuming wind is one-dimensional. This maximum could be reached when the axial induction factor is 1/3.

There are three approaches to increase the power output: first, to improve turbine efficiency, second, to increase the swept area, and last, to operate in a windy environment. However, all these three approaches must meet the safety requirements. It is necessary to balance the benefits and penalties in designing a wind turbine. It must be noted that, for grid-connected wind turbines, like many other power generating devices, grid code must be followed. this should also be a sensitive factor to consider when discussing the overall cost of wind energy project.

The performance of a wind turbine can be compared by power curve and power-tip speed ratio (Cp-λ) curve.

Wind has temporal variations as well as spatial variations. However, it is still possible to find rich wind energy zones on the planet from a long-term measurement and wind resource assessment. Wind maps of different countries can provide important information of macro-siting of wind farm.

Long-term wind statistics can be approximated by a few probability distributions, Weibull distribution and Rayleigh distributions. They reflect the possibility of different wind speed over a long period for instance a year. There are two key factors of the Weibull distribution, one is the shape factor, and the other is the scale factor. Given a measurement from metro masks, Weibull distribution could be generated through tool like WAsP.

The first VAWT is believed to be invented in ancient Persian, for modern development, a notable design is given by a French engineering Darrieus. It was a three-bladed lift driven design. Savonius developed a Bucket shape wind turbine. which is known as drag driven design. Darrieus wind turbine, nowadays, usually refers to lift driven wind turbine.

A series of investigations of VAWT were carried out in the Sandia National Laboratory since 1970s in USA. In Europe VAWT received good reception in UK and Netherlands, as against the Danish type propeller. Musgrove, Giromill, and Helical turbine, and more recently, V-type generator developed by Sharp are some notable examples.

VAWT is rotating across the wind, and thus has a continues change of angle of attack, this feature added to the difficulties of analysing the VAWT rotor.

One the other hand, VAWT has no yaw mechanism, generator could be placed to the ground, and the blade manufacture is easier, this make it a favourable choice of future wind farm.

Modern wind farms are constructed using HAWTs, but VAWT wind farm once existed at Cameron Ridge, Califonia, using the rather successful FlowWind 17m and 19m VAWT, but soon they are replaced by the new trend and by the fast development of HAWT.

One biggest challenge to VAWT is the complex aerodynamics at various scales, blade, rotor and wind farm. At wind farm scales, challenges are wake effects, wake interaction with atmospheric turbulence, while at blade and rotor scales, the challenges are the unsteadiness and vortical flows, flow curvature effects and 3D effects.

2.2 Wake Effects Research: State-of-the-Art

2.2.1 Overview

Wake is treated as an atmospheric boundary layer flow phenomenon. Several orders of magnitude of length scales play an important role in wake development. First one is the atmospheric turbulence scale, characterizing the motion of large atmospheric eddies, it increases linearly with the height of the surface layer. Second one is a wake interface turbulence scale, characterizing the mixing of the wake boundaries with the atmospheric flow, evolved to be in the same order of magnitude of wind turbine rotor diameter. Third one is the turbulence length scale

of the blade induced vortex structure, roughly in the same of order of magnitude of the blade chord length.

A primarily objective of wake effect study is to predict the velocity decay within the wake region. A wake region can be separated into near wake and far wake (see Figure 2-1**Error! Reference source not found.**).

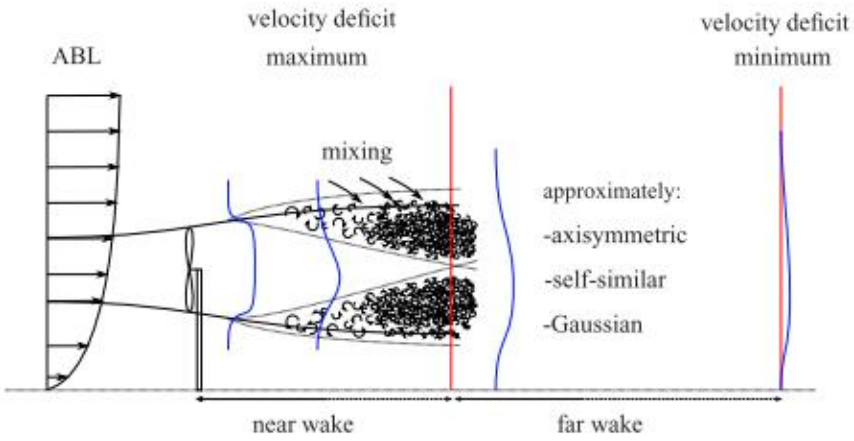

Figure 2-1 Schematic division of wake regions

(source: (Sanderse, 2009))

Classic theory of wake effects indicates a near wake region of 2-4 diameters downstream, and the minimum centreline velocity is reached at 1-2 diameter downstream and recover because of enhanced mixing. Tip vortices decay in 2-3 diameter due the ambient turbulence. There will be an annular shear layer where large scale turbulence formed and spread into the core of the wake, this part of turbulence reaches the centreline at 3-5 diameter downstream. Beyond 5 diameters downstream, the velocity profile is of bell shape and decays monotonically. The axial turbulent velocity (standard deviation of axial velocity) decay with an exponent around -2/3 in most cases. And the length scale of turbulence introduced by the wake is of the order of the rotor diameter.(Ainslie, 1988)

It is worth noting that there is no universally accepted rule to decide how the near and wake region shall be determined. For instance, Crespo et al (Crespo and Hernández, 1996) use 1D to 3D as near wake.

According to wind energy handbook(Burton et al., 2001), Vermeulen proposed a near wake length formula which takes into account the contributions from ambient turbulence, rotor generated turbulence and shear generated turbulence. x_n, the near wake length is

$$x_n = \frac{nr_0}{\left(\frac{dr}{dx}\right)} \tag{2-1}$$

where

$$r_0 = R\sqrt{\frac{m+1}{2}} \tag{2-2}$$

$$m = \frac{1}{\sqrt{1-C_T}} \tag{2-3}$$

$$n = \frac{\sqrt{0.214+0.144m}\left(1-\sqrt{0.134+0.124m}\right)}{\left(1-\sqrt{0.214+0.144m}\right)\sqrt{0.134+0.124m}} \tag{2-4}$$

and dr/dx is the wake growth rate: R is the rotor radius,

$$\frac{dr}{dx} = \sqrt{\left(\frac{dr}{dx}\right)_\alpha^2 + \left(\frac{dr}{dx}\right)_m^2 + \left(\frac{dr}{dx}\right)_\lambda^2} \tag{2-5}$$

where

$$\left(\frac{dr}{dx}\right)_\alpha = 2.5I_0 + 0.005 \tag{2-6}$$

is the growth rate contribution due to ambient turbulence,

$$\left(\frac{dr}{dx}\right)_m = \frac{(1-m)\sqrt{1.49+m}}{(1+m)9.76} \tag{2-7}$$

is the contribution due to shear-generated turbulence,

$$\left(\frac{dr}{dx}\right)_\lambda = 0.012B\lambda \tag{2-8}$$

is the contribution due to mechanical turbulence, where B is the number of blades and λ is the tip speed ratio. (Burton et al., 2001)

To account for the wake added turbulence to the flow, Quarton (Quarton and Ainslie, 1990) proposed the following formula. The wake turbulence is described as a function of wind turbine operating characteristics, ambient wind conditions, and downstream distance from the rotor plane

$$I_{add} = 4.8{C_T}^{0.70}{I_{amb}}^{0.68}(x/x_n)^{-0.57} \quad (2\text{-}9)$$

C_T is the thrust coefficient of the turbine in operation, $I_{amb} = \frac{\sigma}{\overline{U}}$ is the ambient turbulence intensity, σ is the standard deviation of wind speed, $\overline{U}$ is the mean wind speed, x_n is the normalized near wake length, x is the normalized downwind distance.

Wake effects were explored in the IEA Annex IX and more recently IEA Annex XXXI, ENDOW(Rados et al., 2001, Schlez et al., 2001, Barthelmie et al., 2004), UPWIND(Barthelmie et al., 2007), TOPFARM(Larsen and Réthoré, 2013, Réthoré et al., 2011) projects.

The wakes effects research is based on experiments and modelling. This section aims to review the experiments and modelling work about wake effects.

2.2.2 Experiments

Experimental study has played a key role for understanding the wake effects. Many experiment studies can be found mainly for HAWT, ranging from a number of issues, atmospheric stability, meandering.

Hogstrom et al(Högström et al. 1988) conducted a field study of the wake behind a 2MW HAWT using a high resolution Sodar. The measurements were made at several distances between 2D-3.6D. Good quality data of the centreline velocity deficient the longitudinal turbulence intensity was obtained with Tala kites at distances of up to 10.5D. Højstrup et al (1993) made full scale measurement to the wind turbine wake of Nørrekær Enge II. Helmis et al(Helmis et al. 1995) studied the near wake of a single medium-sized wind turbine in Samos Island

wind park. Non-linear interaction of the near wake with the turbine shadowing. Ambient turbulence apparently affects the wake at lower wind speed at distance of 1 rotor diameter. The wake centreline is above the hub height and wake found to be rotating. Ebert et al(Ebert and Wood 1997; Ebert and Wood 1999; Ebert and Wood 2000) described measurements in the near wake of a small HAWT over a range of tip speed ratio. They found angular momentum increase as the tip speed ratio increases. Magnusson (Magnusson 1999) studied the near wake of wind turbines, he pointed out that the atmospheric stratification, the energy extraction, and the yaw angle are three major factors that affect the wake behaviour. Adaramola et al (Adaramola and Krogstad 2011) carried out experimental investigation of wake effects on wind turbine performance and found that the loss in power from the downstream wind turbine varies from about 20%-46% compared to the power output from an unobstructed single turbine operating at its designed conditions. Zhang(Zhang, Markfort, and Porté-Agel 2011) conducted a series of wind tunnel experiment to characterise the structure of the near wake flow downwind of a model wind turbine placed in a neutral stratified boundary layer flow. Vortices were found to last 2-3 rotor diameters downstream. longer than the hub/root vortices in the near wake. Hu, et al(Hu and Du 2009) conducted experimental study of the near wake of a model HAWT, where they found the circumferential component and the radial component of turbulence intensity are higher than that the axial component in the wake region.

While many wake effects experiments can be found about HAWT, very few experimental study work can be found for VAWT.

Bergerles (Bergeles, Michos, and Athanassiadis 1991) studies the near wake of a model VAWT. Mean velocity measurements of VAWT were performed in the wake behind by Sun (Sun, 1981). Goldenberg et al (1983) study indicated rotating VAWT can be spaced more closely due to the wake deflection induced enhanced mixing. Whittlesey, Kinzel and Dabiri et al (Whittlesey, Liska, and Dabiri 2010; Kinzel, Mulligan, and Dabiri 2012; Dabiri, n.d.) field measurements showed the counter rotating VAWT can improve wind farm efficiency.

Compare to HAWT wake effects, the VAWT wake effects are more complicated, due to its unique way of operation. The interaction occurs between the blades and wakes from itself and upstream turbine poses significant engineering challenge.

2.2.3 Modelling

Great research efforts been put into wake modelling. Different wake models have been applied in wake effects analysis. Some early literature review concerning wake effects can be found Bossanyi et al(Bossanyi et al., 1980) Crespo et al (Crespo et al., 1999) Vermeer et al (Vermeer et al., 2003) and Barthelmie(Barthelmie et al., 2006) , Sanderse(Sanderse, 2009) modelling method for wake effects. However, their focus is on the horizontal axis wind turbine wake effects.

Many models have been proposed based on conservation of mass and momentum. Four groups of wake decay models can be found.1. Roughness models. 2. Kinematic models, 3. Field models, 4. Computational fluid dynamics(CFD) models.

Roughness models (Templin, 1974b, Newman, 1977) are a group of model based on the assumption that loss of power in a large wind farm is limited by the equilibrium of atmospheric boundary layer. Wind turbine array are treated as roughness element, the modify wind shear profile based on a combined roughness is then calculated, and velocity at the wind turbine hub height is determined. Though this model is not very popular in modern industry, it is useful for estimating the overall performance of wind farm. Bossanyi et al (Bossanyi et al., 1980) and Milborrow (Milborrow, 1980) made excellent reviews on this type of models.

Kinematic models (Jensen, 1983, Katic et al., 1986) are based on momentum conservation. The flow is treated as negative co-flowing jet. (Lissaman, 1979). The growth rate is calculated as being caused by the ambient turbulence. Because of the simplicity and low computational cost, this model is the most widely used engineering model.

Field models (Crespo and Hernandez, 1986, Crespo et al., 1988, Ainslie, 1985, Ainslie, 1988) calculates velocity from each point based on simplified Navier-Stokes equations. The model assumes that wake of a wind turbine is axisymmetric, fully developed, and not rotating, and can be formulated by time averaged Navier Stokes equation with an eddy viscosity closure. It uses cylindrical coordinates and an assumption of incompressible fluid.

The Increasing in available computational power has led to the a wide application of CFD in wind energy.(Sumner et al., 2010) Based on how the turbulence is resolved, CFD models can be further divided into Large eddy simulation (LES)-based model, and Reynolds-averaged Navier Stokes (RANS)-based model. Although more LES models are used in recent years, its high demand of computing power makes RANS-model a realistic choice. (Réthoré, 2009) Large eddy simulation (LES) can provide higher resolution of temporal and spatial resolution (Porté-Agel et al., 2011). It could be thought as an upgraded version of RANS without using the turbulence closure models, but it uses sub grid scale models to resolve the viscous turbulent flow. RANS method can be an alternative because it is LES computational intensive.

CFD modelling of wake effects has been successfully applied to HAWT (Ivanell, 2009) (Troldborg, 2008). Without physically modelling the wind turbine, Tapia modelled wind flow over complex terrain based on OpenFOAM. Jimenez applied LES model with periodic boundary conditions to simulate the wake and the results indicate that LES is a useful tool to simulate several turbulent characteristics in wakes. Kasmi and Masson introduced a source term accounting for the tip vortices estimated using BEM and tuning the turbulence kinetic energy dissipation equation to model the wake. Rethore modelled the boundary layer using body forces instead of a turbulence model using the Porous disk of body force. Zhang examined the wall function roughness modifications used in Fluent, which describe wall adjacent zone with roughness height but will leads to some undesirable gradient, and he proposed a new remedial wall treatment function to correct the gradient along flow direction. Ammara et al(Ammara et al., 2002) developed a 3D time averaged steady state incompressible Navier-Stokes

equations, and the turbines are represented by surficial forces, are solved using a control-volume finite element method(CVFEM). The 3D method attains the same level of accuracy as the 2-D axisymmetric method and the momentum strip theory. Montavon et al (Montavon et al., 2009) applied CFD model Black Law wind farm based on an actuator disk model, using adaptive gridding to resolve the rotor locations. Stovall et al(Stovall et al., 2010) presented a CFD model base on OpenFOAM to simulate a neutrally stratified atmospheric boundary, where turbine at various downstream positions are located. Both LES and RANS simulations were used. Power deficits ratios for LES and RANS simulations are within 2-4% and 15-43% of experimental data, respectively. Politis et al(Politis et al., 2012) employed k-ω and k-ε turbulence models in modelling the power production from wind farm in complex terrain. Rados et al studied the wake effects using an in-house 3D-NS solver using k-e model and compared the results with experiments and Fluent, it is found that CFD models underestimate the wake effects for the near wake.(Rados et al., 2012) 3D-NS simulation using RNG k-ε turbulence is applied by Ren et al on the NREL 5MW large offshore wind turbine for the distribution characters of the mean velocity. Vafiadis et al(Vafiadis et al., 2013) performed calculate the wake of the Grumman 20kw HAWT based on two commercial CFD codes ANSYS CFX and FLUENT, and the rotor is simplified as disc and behave as momentum sinks. A radially varying thrust coefficient is utilized. Both steady and unsteady computations are carried out.

Three types of CFD models can be found in the far wake modelling. The most detailed is the full-rotor computation (Zahle, 2007). Rotor is resolved without simplification. Detailed information of the flow passing through rotor is retained. An alternative is actuator line method (Sørensen and Shen, 2002, Mikkelsen, 2003) / actuator surface method (Shen et al., 2009). The full rotor is not resolved but simplified as a series of force elements. The forces exerted on the fluid is estimated by using the airfoil definition and geometry of the blades and the local velocity at the rotor disk. This application of this type of method on HAWT wake modelling has been successful, even for multiple wake cases. (Troldborg, 2008). The simplest CFD method to model wake is the actuator disc method. The rotor is simplified as an actuator disc, the forces to the fluid estimated from the rotor

thrust coefficient is distributed over the rotor disc. It is in fact a 1-D model with steady state solution. Albeit the fast solution, one shortcoming of this model is that the vortex structures are not as detail as the actuator line model and the full rotor model.

Turbulence modelling is important, and to improve the prediction accuracy, various effort been made. El Kasmi, et al (El Kasmi and Masson 2008) proposed an extended k-ε model.

Given the cost associated to wake effects field test, CFD modelling might be taken as a cost-effective approach for VAWT wake modelling.

Table 2-1 A List of code for wake effects modelling

Code name	Developer	Models type
WAsP	DTU	Kinematic
Windfarmer	Garrad Hassan	Kinematic, Field model
WindSim	WindSim	CFD
WindPRO	EMD International A/S	Field model, CFD
EllipSys3D	DTU	CFD
3D-NS	RGU	CFD
FlowNS	NTUA, Greece	CFD
FLaP	Oldenburg	CFD
CFDWake	CENER	CFD
Wakefarm	ECN	Field model

A few mathematical models are put forward to described the wake decay effects and some specialized software packages are developed and widely used. Despite of the success of theses wake models, they all failed to discuss the VAWT wake effects. Though some measurements by Liu et al (Liu et al., 1987)

and (Bergeles et al., 1991) have indicated that VAWT wake profile may shift to one side, the wake structure of VAWT and its development are not completely known.

2.3 Aerodynamic Analysis Methods

2.3.1 Overview

Wind turbine aerodynamics are closely linked to turbine energy extraction. To determine the aerodynamics performance of wind turbine is still a challenging issue. Because the wind turbine operating in the bottom of the atmospheric boundary layer, the flow is highly turbulent and unsteady. (Vermeer, Sørensen, and Crespo 2003) The complicate operation of wind turbine needs to perform, such as pitching and yawing, leads to the difficulty of aerodynamics predictions. The aim of this section is to examine the prediction methods of the unsteady aerodynamic loads on wind turbine, especially VAWT.

Many methods have been proposed for wind turbine aerodynamics and they can be grouped into two types. 1) Engineering/Analytical models, 2) Numerical models. Engineering models /Analytical models based on simplified assumptions and without direct solution of Navier-Stokes equations or Lattice Boltzmann equation, while numerical model discretize the flow domain and solve the direct/approximate form of the Navier Stokes equations.

2.3.2 BEM method

BEM is the most commonly used tool for calculating wind turbine forces/loads. It has to be based on airfoil data. Lift and drag are expressed as a function of angle of attack, and Reynolds number which affect the lift and drag coefficient. This model stem from the Momentum/Actuator disc model. An important concept of the model is induction factor.

Assuming a process that cause the velocity to reduce from V_1 to V_2, the ratio between the deficit and the inflow V_1 could always be determined, and we divide this ratio by 2, and name this new ratio as axial induction factor. It is easy to see that the induction factor is an indicator of the capability of converting kinetic energy in that process., the greater the factor is, the more energy is converted from flow, and when the induction factor is negative, it means the process accelerate the fluid, indicating external energy enter the conservative system.

The use of induction factor helps in defining the velocity at different location as a function of inflow velocity. The calculation of aerodynamic forces can suitably switch to the calculation of the induction factor, a coefficient showing energy conversion efficiency of a process. It is not difficult to derive the induced velocity at the rotor plane for one dimensional flow is half of that at the end of control volume.

Templin developed a single stream tube model.(Templin, 1974a), where the VAWT is enclosed in one single stream tube. This model can predict the overall performance of a lightly loaded wind turbine but according to the inquest, it always predicts higher power than the experimental results.(Islam et al., 2008)

Strickland developed a multiple stream tube model(Strickland, 1975),which from the bases of the DART ocde. In this model, induced velocity is found by equating the blade elemental forces (including airfoil drag) and the change in the momentum along each streamtube. (Islam et al., 2008)

Paraschivoiu et al developed the double multiple stream tube model (DMST) (Paraschivoiu, 1982, Paraschivoiu and Delclaux, 1983). in this model the calculation is done separately for the upstream and downstream half cycles of the turbine. (Islam et al., 2008)

The limitation of the BEM model is at high load condition, the assumption of equilibrium which means there is no hysteresis when wind changes. (Snel, 1998, Hansen et al., 2006) So it is not applicable to yaw and pitch control, under the same token, not vertical-axis wind turbine.

The original BEM model is based quasi-steady assumption; This has to be modified when used in time domain dynamic simulation by adopting the dynamic inflow assumption.(Bossanyi, 2003, Hansen et al., 2006)

2.3.3 Vortex method

Vortex model is an alternative to BEM model for obtain aerodynamic forces, it has two variations: free wake assumption (Zervos et al., 1988) or prescribed/fixed wake assumption (Jiang et al., 1991). The method calculates the aerodynamic forces based on the Kutta-Joukowsky theory. The lift is determined by a function of circulation and chord length. The essence of this method is to resolve the vortex field adjacent to the blade element, and resolve the far field through the Biot-Savart equation. Vortex method could be used for highly loaded rotors at high tip-speed ratio. But the angle of attack also needs to be resolved and lift would also rely on a look up table as in the BEM models.

Vortex models were used for helicopter rotor calculations (Bagai et al., 1999, Leishman and Bagai, 1998) In wind energy sector, Strickland (Strickland et al., 1979) developed 2D and 3D vortex method for Darrieus VAWT. Holme (Holme, 1977) conducted analysis for two-dimensional inviscid flow through straight-bladed VAWT, and results show that aerodynamic loading is higher on the upwind side, while streamtube method does not show these features. From shed and bound velocity, the induced velocity is determined from the vorticity sheets, then the angle of attack is also calculated when induced velocity is known.

Panel method could be thought as an extension of vortex method which shares the same wake treatment. It is more efficient in dealing with the highly three-dimensional flow. Panel method are discussed extensively by Dixon (Dixon, 2008, Dixon et al., 2008) and Simão Ferreira. (Simão Ferreira, 2009)

Strictly speaking, both Vortex and panel models based on inviscid flow field, viscous phenomenon like frictions and dynamic stall are not readily reflected in the model. But they are considered by look up table and empirical dynamic stall model, e.g. the Gormont model (Gormont, 1973) and Leishman-Beddoes model. (Leishman and Beddoes, 1989)

Kecskemety et al (Kecskemety and McNamara, 2010) developed a free wake model based on a time marching vortex line method. the model is used to examine the time step required to capture the effect of inflow turbulence. The recommended time step size is 10° in azimuthal angle.

Vortex model is an alternative to BEM model for obtain aerodynamic forces, it has two variations: free wake assumption(Zervos et al., 1988) or prescribed/fixed wake assumption(Jiang et al., 1991). The method calculates the aerodynamic forces based on the Kutta-Joukowsky theory. The lift is determined by a function of circulation and chord length. The essence of this method is to resolve the vortex field adjacent to the blade element, and resolve the far field through the Biot-Savart equation. Vortex method could be used for highly loaded rotors at high tip-speed ratio. But the angle of attack also needs to be resolved and lift would also have to rely on a look up table as in the BEM models.(Vermeer et al., 2003)

Vortex models were used for helicopter rotor calculations (Bagai et al., 1999, Leishman and Bagai, 1998) In wind energy sector, Strickland(Strickland et al., 1979) developed 2D and 3D vortex method for Darrieus vertical-axis wind turbine. Holme (Holme, 1977)conducted analysis for two-dimensional inviscid flow through straight-bladed VAWT, and results show that aerodynamic loading is higher on the upwind side, while streamtube method does not show these feature. From shed and bound velocity, the induced velocity is determined from the vorticity sheets, then the angle of attack is also calculated when induced velocity is known.

Panel method could be thought as an extension of vortex method which shares the same wake treatment. It is more efficient in dealing with the highly three-dimensional flow. Panel method are discussed extensively by Dixon(Dixon, 2008, Dixon et al., 2008) and Simão Ferreira.(Simão Ferreira, 2009)

Strictly speaking, both Vortex and panel models based on inviscid flow field, viscous phenomenon like frictions and dynamic stall are not readily reflected in the model. But they are considered by look up table and empirical dynamic stall

model, e.g. the Gormont model(Gormont, 1973) and Leishman-Beddoes model.(Leishman and Beddoes, 1989)

Table 2-2 List of aerodynamic analysis tools

Author	Model name	Model type
Van Bussel (Van Bussel, 1992)	PREDICHAT/PREDICDYN	BEM
Deglaire (Deglaire, 2010)	Semi-Analytical	Vortex
Ponta (Ponta and Jacovkis, 2001)	FEVDTM	Vortex
Strickland	VDART3	Vortex
Paraschivoiu	CARDAA	BEM
Paraschivoiu	CARDAAX	BEM
Shires	TM	BEM
Allet	3DVF	BEM
Paraschivoiu	CARDAAS	BEM
Paraschivoiu	CARDAAX	BEM
Strickland	DART	BEM
Strickland	VDART2	Vortex

2.3.4 CFD method

CFD is a numerical method used in both near wake and far wake investigation.

CFD method has been used widely in wind industry to predict the wind turbine performance.(Sumner et al., 2010) However, it is still a non-trivial task to obtain full image in the field, due to the highly complex physics it has to solve and the computational resources that are available. CFD serves as an alternative to experiment and theory when they are not available. (see Figure 2-2 **Error! Reference source not found.**)

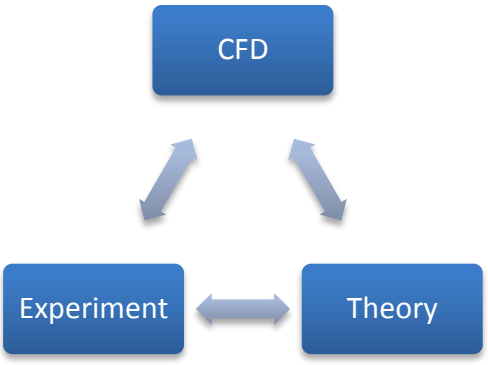

Figure 2-2 Role of CFD

There are also many variations in CFD methods, such as Reynolds-Averaged Navier Stokes(RANS), Large Eddy Simulation (LES), Direct Numerical Simulation(DNS), Lattice Boltzmann Method(LBM). It is worth mentioning that for the LBM, instead of solving the Navier-Stokes equations, the discrete Boltzmann equation is solved to simulate the flow of a Newtonian fluid with collision models.

RANS has been used to study the wind turbine aerodynamics by many researchers as reviewed by Sumner et al(Sumner et al., 2010) The turbulence closure models play a very important role in the accuracy of RANS simulation.

McLaren et al (McLaren et al., 2012) use RANS to simulate the aerodynamics performance of a high solidity VAWT, and Qin et al (Qin et al., 2011) applied RANS solver to studied the dynamic stall of VAWT blade.

To simulate the time dependent properties in the flow, it is helpful to further divide the RANS into Steady/Time independent RANS and Unsteady/Time dependent RANS. The latter solution will march overtime so it can facilitate analysis for wind turbine in rotation.

Large eddy simulation (LES) can provide higher resolution of temporal and spatial resolution(Porté-Agel et al., 2011). It could be thought as an upgraded version of RANS without using the turbulence closure models, but it uses sub grid scale models to resolve the viscous turbulent flow.

Direct Numerical Simulation (DNS) is even more challenging and require more computational resources to resolve the viscous flow as it does not rely on

turbulence closure model or subgrid(SGS) scale models instead it solves the Navier stokes equations directly, and all the spatial scales of the turbulence will be solved, hence it has the highest solution. But it also means it requires more computational resources than RANS and LES.

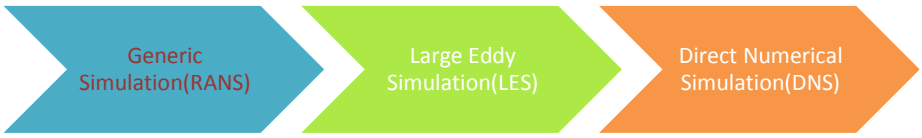

Figure 2-3 Different types of CFD Methods

2.4 CFD on STAR-CCM+

2.4.1 Overview

Many CFD tools are available. The commercial CFD package being used for the current research is STAR-CCM+, developed by CD-Adapco. It provides the world's most comprehensive engineering physics simulation inside a single integrated package, and it also provides a suite of integrated components that combine to produce a powerful package that can address a wide variety of modelling needs. STAR-CCM+ became the first commercial CFD package to mesh and solve a problem with over one billion cells.

Advanced automatic meshing technology generates either polyhedral or predominantly hexahedral control volumes at the touch of a button, offering a combination of speed, control, and accuracy.

An important part of mesh generation for accurate CFD simulation is the near-wall region, or extrusion-layer mesh. STAR-CCM+ automatically produces a high-quality extrusion layer mesh on all walls in the domain.

It has a comprehensive range of turbulence models: k- ε model (Standard, V2F, Realizable, Two-layer); k-ω model (Standard, SST and BSL); Reynolds stress model (RSM-linear and quadratic); Spalart-Allmaras model.

It is one of the leading CFD tools designed for multi-disciplines, and one merit of it is that it can be operated on the High-Performance Computing (HPC) platform

for up to 32 processors at Cranfield University, which boosts the performance especially for very large and complicated case.

Another advantage of using STAR-CCM+ is that it also can perform Detached Eddy Simulation (DES) and Large Eddy Simulation (LES), although by default all the simulation is run on Reynolds Averaged Navier-Stokes (RANS) solvers along with different turbulence models.

2.4.2 Governing equations

Although use of LES is slowly increasing, most models are based on the Reynolds-Averaged Navier-Stokes (RANS) equations, especially for aerodynamic performance prediction. A correct solution of the boundary layer flow is essential to the aerodynamic prediction. The flow regime in a boundary layer can be laminar, or turbulent depending on the Reynolds number.

Apart from the viscosity in laminar flow, for turbulent flow, there is an extra viscosity for viscous flow. Resolving this turbulent viscosity is the task of many turbulent closure models.

The solution of Reynolds-averaged Navier-Stokes equation, requires the solutions of the viscous stress tensor $\mathbf{T}$

$$\mathbf{T} = \mathbf{T}_l = \mu\left[\nabla\mathbf{V} + \nabla\mathbf{V}^{\mathbf{T}} - \frac{2}{3}(\nabla\cdot\mathbf{V})\boldsymbol{I}\right] \tag{2-10}$$

$\mathbf{T}$ is the viscous stress tensor, $\mathbf{V}$ is velocity vector,

and for turbulent flow:

$$\mathbf{T} = \mathbf{T}_l + \mathbf{T}_t \tag{2-11}$$

The subcripts denote the flow regime,and according to the Boussinesq approaximation:

$$\mathbf{T} = \mu_{eff}\left[\nabla\mathbf{V} + \nabla\mathbf{V}^{\mathbf{T}} - \frac{2}{3}(\nabla\cdot\mathbf{V})\boldsymbol{I}\right] \tag{2-12}$$

where the effective viscosity is

$$\mu_{eff} = \mu + \mu_t \tag{2-13}$$

Based on Reynolds averaging, the turbulent stress tensor has the following form (without Boussinesq approximation) :

$$\mathbf{T}_t \equiv -\rho\overline{V'V'} = -\rho\begin{bmatrix} \overline{u'u'} & \overline{u'v'} & \overline{u'w'} \\ \overline{u'v'} & \overline{v'v'} & \overline{v'w'} \\ \overline{u'w'} & \overline{v'w'} & \overline{w'w'} \end{bmatrix} \tag{2-14}$$

For eddy viscosity type of turbulent model

$$\mathbf{T}_t = 2\mu_t \boldsymbol{S} - \frac{2}{3}\left(\mu_t \nabla \cdot \mathbf{V} + \rho k\right)\boldsymbol{I} \tag{2-15}$$

k is the turbulent kinetic energy, and $\boldsymbol{S}$ is the strain tensor:

$$\boldsymbol{S} = \frac{1}{2}\left(\nabla\mathbf{V} + \nabla\mathbf{V}^{\mathbf{T}}\right) \tag{2-16}$$

2.4.3 Mesh generation

STAR-CCM+ contains tools which can be used to generate a volume mesh stating from a surface. The entire mesh can be generated directly from within STAR-CCM+.

The core volume mesh can contain either trimmed, polyhedral or tetrahedral type cells for each mesh region, determined using the selection of mesh models. Prismatic cell layers can be included next to wall boundaries and interfaces by using the prism layer or advancing layer meshing models Volumetric controls using such shapes as rectangles (bricks) and spheres can also be included to increase or decrease the mesh density of both the core mesh and/or prism layer mesh. In the case of trimmed cells, automatic feature refinement is included to further optimize the cell distribution through the mesh.

The trimmed cell mesher provides a robust and efficient method of producing a high-quality grid for both simple and complex mesh generation problems.

The resulting mesh is composed predominantly of hexahedral cells with trimmed cells next to the surface. Trimmed cells are polyhedral cells but can usually be recognized as hexahedral cells with one or more corners and/or edges cut off.

Volumetric controls can also be included to locally increase or decrease the mesh density in the template based on a range of prescribed shapes.

The current implementation of the trimmer model is restricted to one region per continua. In other words, a different mesh continuum must be used for each region you have, or alternatively, the per-region meshing option can be activated to apply the same continuum to all regions independently. However, in this way, a conformal trimmed mesh across the interface is not guaranteed, and interfaces can only be used when boundaries in the interface belong to the same region.

Mesher is not able to generate two-dimensional meshes. STAR-CCM+ provided two ways: 1) Create a true two-dimensional mesh and import it directly into STAR-CCM+, Gridgen mesh generator, for instance supports two-dimensional meshes.

2) Create a three-dimensional or quasi-three-dimensional mesh and extract a two-dimensional mesh from it. When importing a 3D mesh that is to be used to create 2D mesh from it, it is important to align and position the mesh correctly such that the desired 2D boundary plane is at Z=0. The extracted two-dimensional mesh is always one meter in depth.

2.4.4 Turbulence models

$\mathrm{Splalart}-\mathrm{allmaras}$ model is a one-equation model. It was designed specifically for aerospace applications involving wall-bounded flows and has been shown to give good results for boundary layers subjected to adverse pressure gradients. It is also gaining popularity in turbomachinery applications. The standard form of $\mathrm{Splalart}-\mathrm{allmaras}$ model is a low-Re model, which means the it requiring the viscous affected region has to be solved. In other words, the wall y+ value has to be need to be close to 1, the mesh has to be very fine close the boundary, to make sure the first layer of the grid lies in the viscous sublayer.

In Spalart – Allmaras model, the turbulent viscosity is express as a function of a viscosity like variable $\tilde{v}$, the formula to resolve is shown blow:

$$\mu_t = \rho\tilde{v}f_{v1} \tag{2-17}$$

$$\nu_t = \mu_t/\rho = \tilde{v}f_{v1}$$

$$f_{v1} = \frac{\chi^3}{\chi^3 + {C_{v1}}^3} \tag{2-18}$$

$$\chi \coloneqq \frac{\tilde{\nu}}{\nu} \tag{2-19}$$

$$\frac{\partial\tilde{v}}{\partial t} + u_j\frac{\partial\tilde{v}}{\partial x_j} = c_{b1}\tilde{S}\tilde{v} - c_{w1}f_w\left(\frac{\tilde{v}}{\tilde{d}}\right)^2 + \frac{c_{b2}}{\sigma}\frac{\partial\tilde{v}}{\partial x_k}\frac{\partial\tilde{v}}{\partial x_k} + \frac{1}{\sigma}\frac{\partial}{\partial x_k}\left[(\nu+\tilde{v})\frac{\partial\tilde{v}}{\partial x_k}\right] \tag{2-20}$$

$$\tilde{S} \equiv S + \frac{\tilde{\nu}}{\kappa^2 d^2}f_{v1} \tag{2-21}$$

$$f_{v2} = 1 - \frac{\chi}{\chi f_{v1} + 1} \tag{2-22}$$

$$S \equiv \sqrt{2\Omega_{ij}\Omega_{ij}} \tag{2-23}$$

$$\Omega_{ij} \equiv \frac{1}{2}\left(\frac{\partial u_i}{\partial x_j} - \frac{\partial u_j}{\partial x_i}\right) \tag{2-24}$$

$$f_w = g\left[\frac{1+{c_{w3}}^6}{g^6+{c_{w3}}^6}\right]^{\frac{1}{6}} \tag{2-25}$$

$$g = r + c_{w2}(r^6 - r) \tag{2-26}$$

$$r \equiv \frac{\tilde{\nu}}{\tilde{S}\kappa^2 d^2} \tag{2-27}$$

$$c_{b1} = 0.1355,\ c_{b2} = 0.622,\ c_{v1} = 7.1, \sigma = \frac{2}{3}$$

$$c_{w3} = 2,\quad c_{w2} = 0.3, \kappa = 0.41,\quad c_{w1} = \frac{c_{b1}}{\kappa} + \frac{(1+c_{b2})}{\sigma}$$

Realizable $k-\varepsilon$ Two-layer model is a modification of the original $k-\varepsilon$ model(Launder and Spalding 1974). it combines the $k-\varepsilon$ model with the two-layer approach. The coefficients in the models are identical, but model gains added flexibility of an all y+ wall treatment. All y+ treatment can emulate the high y+ wall treatment for coarse mesh, and the low y+ wall treatment for the fine mesh.

The eddy viscosity in $k-\varepsilon$ model is expressed as a function of turbulent kinetic energy k and the turbulent dissipation rate ε, see (2-28**Error! Reference source not found.**) and two set of transport equations will be solved for k and ε respectively

$$\mu_t = \rho C_\mu \frac{k^2}{\varepsilon} \tag{2-28}$$

For solution of k:

$$\frac{\partial k}{\partial t} + u_j \frac{\partial k}{\partial x_j} = \tau_{ij} \frac{\partial u_i}{\partial x_j} - \varepsilon + \frac{\partial}{\partial x_j}\left[(\nu + \nu_T/\sigma_k)\frac{\partial k}{\partial x_j}\right] \tag{2-29}$$

For solution of ε

$$\frac{\partial \varepsilon}{\partial t} + u_j \frac{\partial \varepsilon}{\partial x_j} = C_{\varepsilon 1}\frac{\varepsilon}{k}\tau_{ij}\frac{\partial u_i}{\partial x_j} - C_{\varepsilon 2}\frac{\varepsilon^2}{k} + \frac{\partial}{\partial x_j}\left[(\nu + \nu_T/\sigma_\varepsilon)\frac{\partial k}{\partial x_j}\right] \tag{2-30}$$

A notable difference of the Realizable $k-\varepsilon$ model from the standard $k-\varepsilon$ model is that the constant C_μ is not a constant, and C_μ is defined as

$$C_\mu = \frac{1}{A_0 + A_s U^{(*)}\frac{k}{\varepsilon}} \tag{2-31}$$

$$U^{(*)} \equiv \sqrt{S{:}S - W{:}W} \tag{2-32}$$

$$A_0 = 4.0 \tag{2-33}$$

$$A_s = \sqrt{6}\,\cos\phi \tag{2-34}$$

$$\phi = \frac{1}{3}acos\left(\sqrt{6}W\right) \tag{2-35}$$

$$W = \frac{S_{ij}S_{jk}S_{ki}}{\sqrt{S_{ij}S_{ij}}^3} \tag{2-36}$$

$C_{\varepsilon 1} = \max\left(0.43, \frac{\eta}{\eta+5}\right),\ C_{\varepsilon 2} = 1.9,\ \sigma_k = 1.0,\ \sigma_\varepsilon = 1.2,\ \ \eta = \frac{Sk}{\varepsilon}$

SST $k-\omega$ turbulence model is a two-equation model that use the $k-\omega$ model in the inner part of the boundary layer and blended into $k-\varepsilon$ model in the free stream. This is to avoids the common problem of $k-\varepsilon$ being too sensitive to inlet free stream turbulence properties. It shows good behaviour in adverse pressure gradients and separating flow. Like the realizable two layer $k-\varepsilon$, all y+ wall treatment is also available.

For standard $k-\omega$ turbulent viscosity is defined by the turbulent kinetic energy k and a specific dissipation rate ω

$$\mu_t = \rho\frac{k}{\omega} \tag{2-37}$$

For SST $k-\omega$ model

$$\mu_t = \frac{\rho\alpha_1 k}{\max(\alpha_1\omega, SF_2)} \tag{2-38}$$

For solution of k

$$\frac{\partial k}{\partial t} + u_j\frac{\partial k}{\partial x_j} = \mathrm{P}_k - \beta^* k\omega + \frac{\partial}{\partial x_j}\left[(\nu + \nu_T\sigma_k)\frac{\partial k}{\partial x_j}\right] \tag{2-39}$$

For solution of ω

$$\frac{\partial \omega}{\partial t} + u_j\frac{\partial \omega}{\partial x_j} = \alpha S^2 - \beta\omega^2 + \frac{\partial}{\partial x_j}\left[(\nu + \nu_T\sigma_\omega)\frac{\partial \omega}{\partial x_j}\right] + 1(1-F_1)\sigma_{\omega 2}\frac{1}{\omega}\frac{\partial k}{\partial x_i}\frac{\partial \omega}{\partial x_i} \tag{2-40}$$

$$F_2 = tanh\left[\left[max\left(\frac{2\sqrt{k}}{\beta^*\omega y}, \frac{500\nu}{y^2\omega}\right)\right]^2\right] \tag{2-41}$$

$$\mathrm{P}_k = min\left(\tau_{ij}\frac{\partial u_i}{\partial x_j}, 10\beta^* k\omega\right) \tag{2-42}$$

$$F_1 = tanh\left\{\left\{min\left[max\left(\frac{\sqrt{k}}{\beta^*\omega y}, \frac{500\nu}{y^2\omega}\right), \frac{4\sigma_{\omega 2}k}{CD_{k\omega}y^2}\right]\right\}^4\right\} \tag{2-43}$$

$$CD_{k\omega} = max\left(2\rho\sigma_{\omega 2}\frac{1}{\omega}\frac{\partial k}{\partial x_i}\frac{\partial \omega}{\partial x_i}, 10^{-20}\right) \tag{2-44}$$

$$\phi = \phi_1 F_1 + \phi_2(1 - F_1) \tag{2-45}$$

$$\beta^* = 0.09$$

2.5 Summary

In this chapter, literature from various subjects is reviewed, focusing on mainly three different aspects: the development of wind energy technology, wake effects research, and the aerodynamic analysis methods for wind turbine. In addition, the tool selected for the study, STAR-CCM+, is introduced. Some key points can be drawn from the literature review.

Wind energy grows rapidly and requires technology innovation to bring down cost, and VAWT is a potential option for future wind farm.

Many projects about wake effects were carried out in the past, however, they overlooked the study of VAWT wake effects.

CFD have been used extensively for study the wind turbine aerodynamics and HAWT wake effects, it is useful method to study the VAWT wake effects. RANS method is a less expensive method can be used for modelling wake effects compared to LES and DNS.

STAR-CCM+ is an advanced CFD tool readily available for the task, with a range of turbulence models and relative strong mesh generation capability.

3 NEAR WAKE MODELLING

3.1 Introduction

The objective of near wake modelling is to determine the aerodynamic performance of VAWT under various inflow conditions. Different cases that are closely linked to the aerodynamics performance of VAWT will be studied. Aerodynamics of a circular cylinder, airfoil and a VAWT rotor are modelled using RANS method.

Challenges in this section is to model the rotor wake and the unsteady aerodynamics of VAWT. Investigations of the near wake of full-scale turbines are needed to generalise the results from far wake measurements on these machines.

3.2 Cylinder Wake Modelling

3.2.1 Overview

Cylinder wake is one of the most revealing cases in fluid mechanics. Karman vortex street is a classic example of vortex shedding, flow separations can happen on the surface of a cylinder, and dynamic pressure force on the cylinder introduced flow is an important design parameter for structural design.

According to the theory of similarity and dimension analysis, Reynolds number is dimensionless factor indicating the ratio of inertial force to viscous force, it provides a means to compare the viscous effects of fluid on similar geometry but in various size. The Reynolds number concept is used for both internal flow such as fluid in a pipe and external flow such as flow surround wing body. Reynolds number is used as a threshold in internal flow study to distinguish turbulent and laminar fluid regime. Two critical Reynolds number can be defined in internal flow, the upper critical Reynolds number $Re_{cr'}$, where at a greater Re than this point the flow becomes turbulent, and lower critical Reynolds number Re_{cr}, where at a smaller Re this point the flow is laminar. The Re between the two critical Reynolds number are not stable, a small perturbation of low could turn the laminar flow to turbulent. In engineering practice, the lower critical Reynolds number is 2320,

and the upper critical Reynolds number can be as high as 13800, but since the flow is prone to perturbation in the region between the two number, it is generally accepted in engineering that $Re = 2000$ is the criterion to tell laminar flow from turbulent flow. However, this criterion is less pronounced in external flow. A jet flow could be either laminar of turbulent, on example of this is the smoke coming out from chimney.

Laminar flow is defined as a flow in which the streamlines are smooth and regular and a fluid element moves smoothly along a streamline, while turbulent flow is a flow which the streamline break up and a fluid element moves in a random irregular and tortuous fashion. Turbulent profile is fatter than the laminar profile, and have a stronger lateral momentum exchange. Laminar shear stress is less than the turbulent shear, indicating a smaller skin friction on a body surface and smaller friction drag. Similar trend can be observed in heat transfer on body surface, and turbulent aerodynamic heating is stronger than laminar aerodynamic heating.

For external flow, local Reynolds number concept is used to determine the development of a boundary surface, the length scale is represented by a distance from the leading edge. A critical Reynolds number can also be defined indicating the laminar and turbulence transition for boundary layer development for external flow. Assuming flow is laminar from the leading edge of a plate, at some point downstream of the plate, laminar boundary layer will grow and become unstable, with small turbulent eddies turn to a transition region before fully turbulent. The point at which the boundary layer become fully turbulent is known as the transition point, and the distance from transition point to leading edge is known as the critical distance, the Reynolds number defined based on this critical distance is the critical Reynolds number, an indicator of determine the boundary transition. Shape of geometry and surface roughness will affect the location as well. They can be determined through experiment or semi-empirical theory. Knowing the critical Reynolds number, the transition point of boundary layer surface could then be calculated. The location of transition point will affect the skin friction integration

because of reason mentioned before, thus, it is important to friction drag prediction.

Drag on a body is of great engineering importance, for a two-dimensional body, friction drag and pressure drag, and induce drag for a finite wing body(3D). Fully attached flow will have no pressure drag, and when the flow separation happens, pressure drag will be introduced due to the unbalance pressure body. To predict the flow separation and pressure distribution accurately therefore is important.

Modelling flow separation is important step for understanding the force distribution around the surface of a body. The viscosity the turbulence geometry shape and surface roughness will affect the transition point contributing the friction, and flow separation will affect the pressure drag, and the vortex structure around the body will also change according.

Vortex structure of fluid surround bluff body has long been a key to understand the fluid dynamics of the body. However, bluff body vortex structure is complex because it involves the interaction of three components in the same problem, boundary layer vortices, separating free shear layer vortices, and wake vortices. Bluff body wake flows have direct engineering significance. The alternate shedding of vortices in the near wake, in the classical vortex street configuration, leads to large fluctuating pressure forces in a direction transverse to the flow and may cause structural vibrations, acoustic noise, or resonance, which in some cases can trigger failure. Wake structure of bluff body has been investigated in past in either 2D and 3D, and nominal 2D wake could possess 3D aspect, a comprehensive review about these 3D effects are reviewed by Williamson (Williamson, 1996)

Among many others, the GALCIT experiment is one experiment to investigate the vortex structure around a cylinder. The Reynolds number is 140,000, a low enough Reynolds number to insure a laminar separation, and high enough to insure a fully turbulent wake, in other words, flow separation will happen before the transition point is formed. It has been used as a test case for some advanced calculation codes. (Cantwell, 1976) and it is used as one of the collaborative data sets for RANS turbulence modelling validation.

This Reynolds number can happen to some critical components of VAWT, such as tower and supporting arms. For example, the tower diameter of the Sandia 17m is 0.762m, and assuming a velocity of 2.7m/s and use the standard dynamic viscosity and density of air. The tower will likely experience same fluid dynamics process as the cylinder in GALCIT experiment. This wind speed can be a representative wind speed for a parked wind turbine if the cut-in wind speed is 3.0m/s as set for many HAWTs.

Therefore, the experiment settings were recreated on a commercial CFD package. The objectives of simulation are two-folded: one is to verify the commercial CFD code and its sub models, and the other is to understand the vortex structure formation and transportation in the near wake of a cylinder.

The original experiment was performed in a 10-foot wind tunnel. Detailed experiment configurations could be found in Cantwell thesis (Cantwell, 1976). A summary is list in the table below. The original circular cylinder used in the experiment is 297.2 cm long, made of stainless steel. The cylinder diameter is 10.137 cm. Two end plates of 60.96 cm in diameter were used to reduce the adverse effects of the tunnel boundary layer. The cylinder was located 15.24 cm above the centreline of the tunnel and 60.96 cm downstream of the leading edge of the test section. The free stream turbulence level was found to be less than 0.6%. To satisfy the Reynolds number, wind speed for the experiment is 21.2 m/s. The Strouhal number for the experiment is 0.179. The shedding frequency therefore can be calculated by definition, which is 26ms, and the drag coefficient is 1.227.

The static pressure was always slightly below atmospheric pressure, the critical Re number appears at 239000 for the cylinder. (Cantwell, 1976), vortex formation region X/D =2.3 and fraction of circulation injected into the wake at one separation points during one shedding cycle which is carried downstream is given by Roshko (Roshko, 1954) on the drag and shedding frequency of two dimensional bluff bodies. NACA TM 3169. $\Gamma = \frac{1}{m^2}\left(1 - \left(\frac{U_{local}}{U_\infty}\right)^2\right), m = \frac{U_S}{U_\infty}$. where U_S is the velocity outside the boundary layer at the separation point.

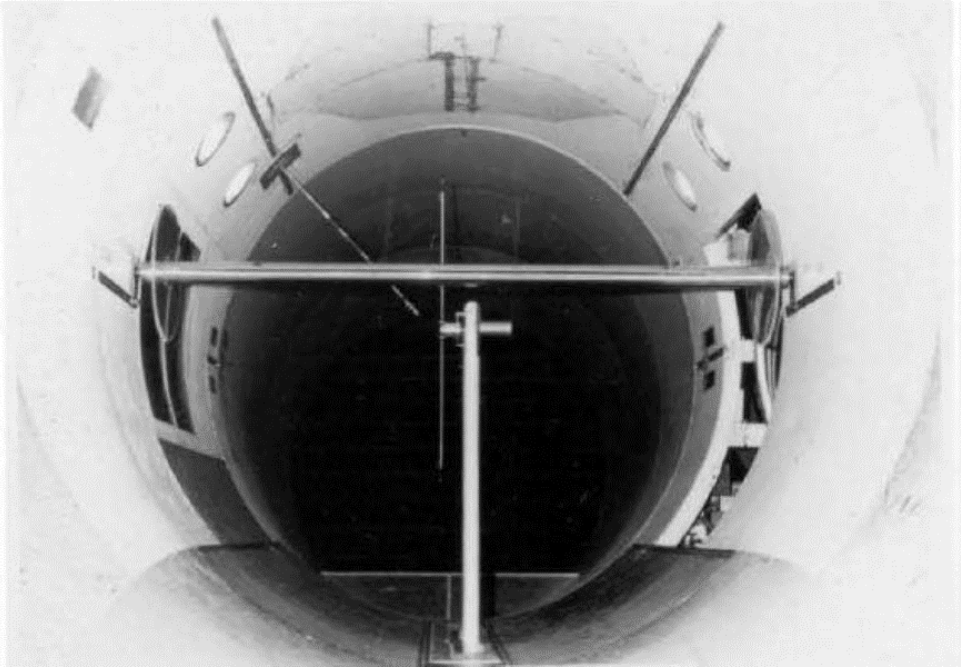

Figure 3-1 GALCIT Wind Tunnel

(source: (Cantwell, 1976))

Table 3-1 Configuration of GALCIT Experiment

Cylinder diameter	0.10137 m
Dynamic pressure	260.65Pa
Free stream speed	21.20±0.10 m/s
Kinematic viscosity	0.1535cm^2/s
Reynolds number	140,000
Shedding period	26.65ms
Strouhal number	0.179
Free stream temperature	24±2 °C
Free Stream turbulence level	≤0.006

3.2.2 Simulation setup

Mesh is created in 3D and then converted to 2D mesh in an application using an integrated module. Mesh is diagnosed and to ensure that there is no negative volume before conversion. A schematic of the mesh is depicted below.

Structured trimmed mesh is used and a cone shape refinement region is added to capture the wake.

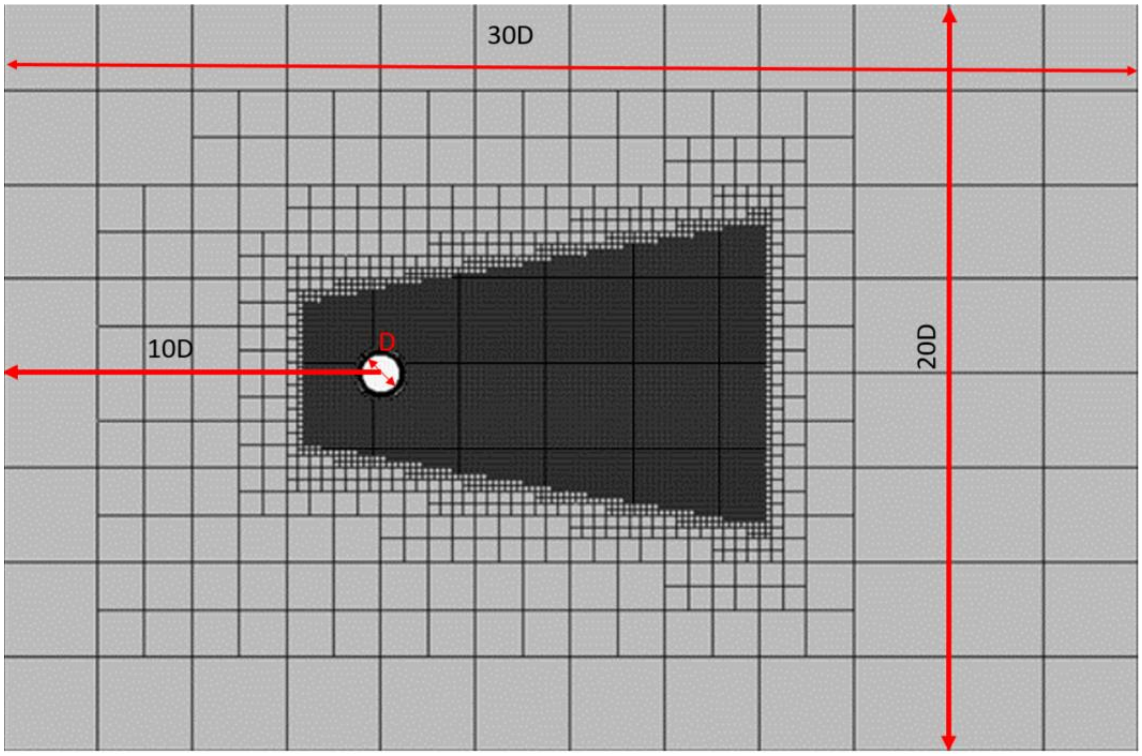

Figure 3-2 2D mesh for modelling cylinder wake

Time step is set to 0.001s so it is estimated 26 time steps, and for each time step, the residuals of the governing equation is set to lower than 10^{-4}. For one unsteady solution, it is very time consuming. But because the inner iteration converged well, the under-relaxation factor of the segregate model solver is changed to speed up the simulation.

The near wall prism layer thickness is 2.7E-5m, to maintain surface wall y+ value between 1 and 2(See Figure 3-3). This is because a wall y+ value close to 1 is recommended by STAR-CCM+ to capture the fully separation for the SST k-ω turbulence model if all y+ treatment is not applied.

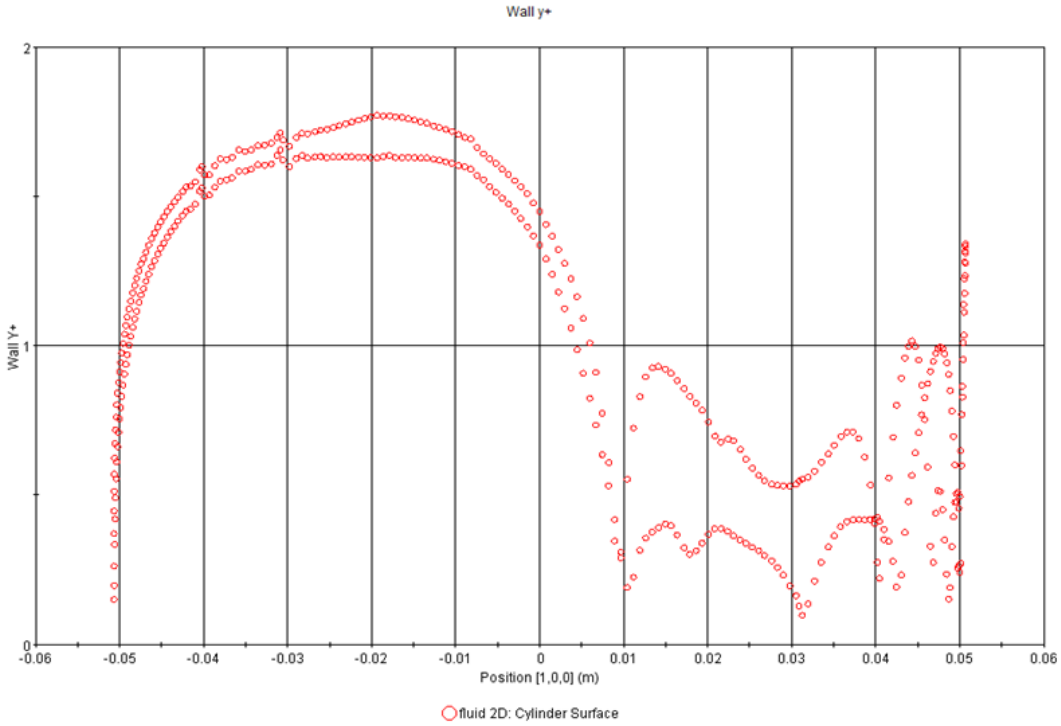

Figure 3-3 Wall Y+ value check in 2D

A mesh sensitivity analysis is carried out. By changing the based size of the model, mesh with different cell count is generated. The maximum lift coefficient is chosen to compared the prediction. Results are shown below in Table3-2. The predicted maximum lift is stabilized near 1.50 despite number cell counts increases.Therefore the selected mesh with a base size 1m is adopted.

Table 3-2 2D Mesh sensitivity analysis

ID	2D cell count	Base size	Cl
Mesh 1	13311	1.0m	1.49
Mesh 2	26735	0.8m	1.52
Mesh 3	5246	1.2m	1.25

2D solution of the same geometry on five different turbulence models are explored. The simulation converged approximately at 180th time step, surface

pressure, velocity and vorticity data were extracted from 200th time step until 260th time step at each time step.

3.2.3 Results and discussion:

In order to assess the simulation results, velocity, frequency and surface pressure are selected to compare with the experiment data and simulation results from other researchers (Song and Yuan, 1990)

Velocity contour of five different turbulence models are listed in Table 3-3. All five models can capture the vortex street shed from the cylinder, and a clearly alternating near wake is observed. Strong vortex is formed and shed near the boundary layer, rolls along the edge of the boundary layer and shed downstream. The RST model and SST k-ω models predict a more lingering vortex zone, while vortex in the laminar, Spalart-Allmaras, and realizable k-ε models are more easily to break down. Despite the relatively coarse time step, 21 ms period is obtained from the lift coefficient history, this is a fair agreement with the observed 26ms from the GALCIT experiment.

Time averaged surface pressure solved by Laminar model is depicted in Figure 3-4, together with the result from GALCIT and the LES simulation results from Song and Yuan. The flow separation point predicted by the RANS method is close that predicted by the LES method.

Velocity data were taken by a series of line probes downstream. one group of probes(as shown in Figure 3-5) is used to measure the velocity deficit distribution at 8 different locations up to 3 diameters downstream. Velocity deficit is compared with the experiment data see Figure 3-6. The laminar simulation tend to over predict the near wake until 3 diameter downstream.

Another line probe as shown in Figure 3-7 is used to measure the centreline velocity. Instantaneous centreline velocity and time averaged centerline velocity are shown in Figure 3-8. Averaged centerline velocity derived from solutioin based on the SST k-ω and laminar model are compared with the experiment data and LES results respectively in Figure 3-9. Turbulent model predicts a much quicker velocity recovery behind the cylinder before 2 diameter downstream,

while laminar model results are in good agreement with the experiment data and LES simulation results.

Table 3-3 Cylinder vorticity contour of five models

Laminar	$Realizable\ k - \varepsilon$	$SST\ \ k - \omega$	RST	Spalart-Allmaras
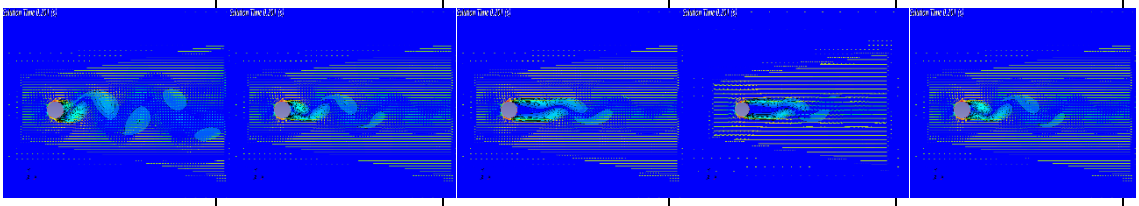				
T=0.201s	T=0.201s	T=0.201s	T=0.201s	T=0.201s
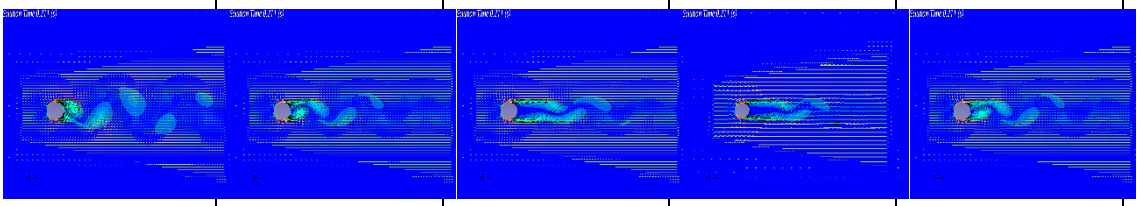				
T=0.211s	T=0.211s	T=0.211s	T=0.211s	T=0.211s
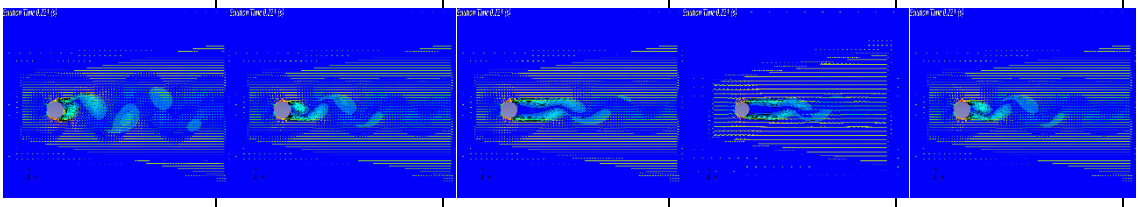				
T=0.221s	T=0.221s	T=0.221s	T=0.221s	T=0.221s
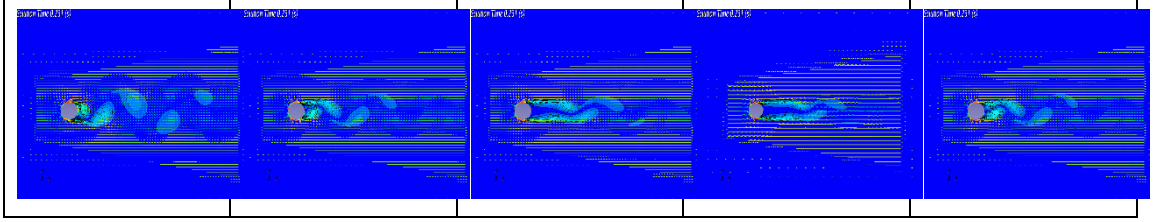				

T=0.231s	T=0.231s	T=0.231s	T=0.231s	T=0.231s

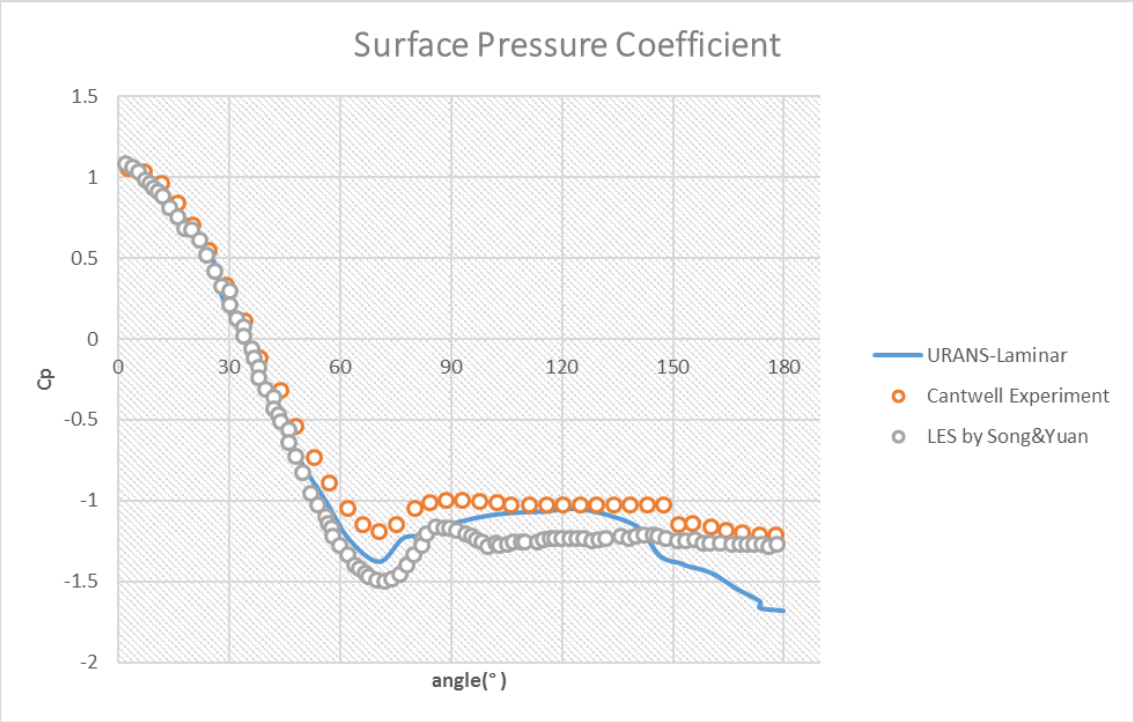

Figure 3-4 Cylinder surface pressure prediction

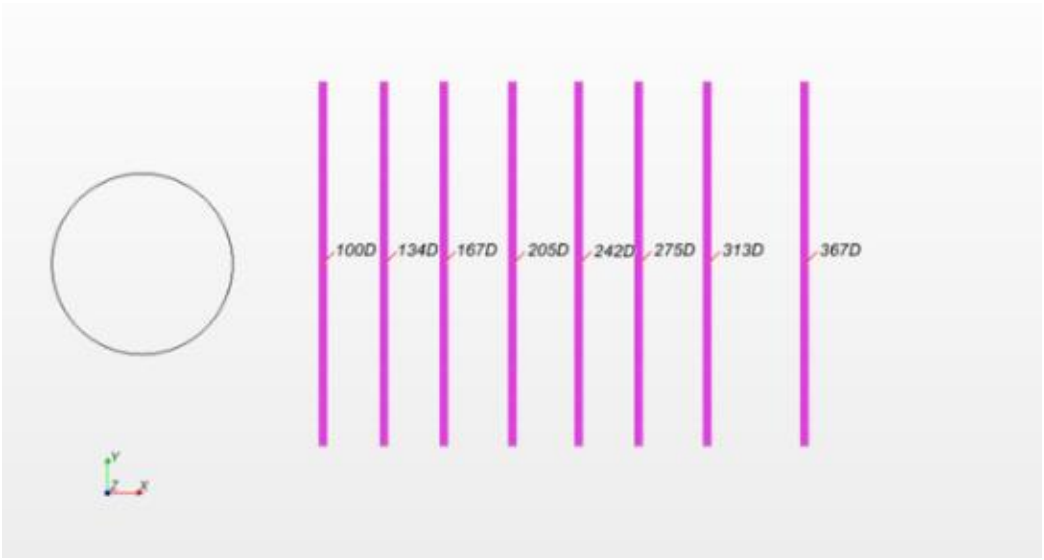

Figure 3-5 Line probes for wake profile

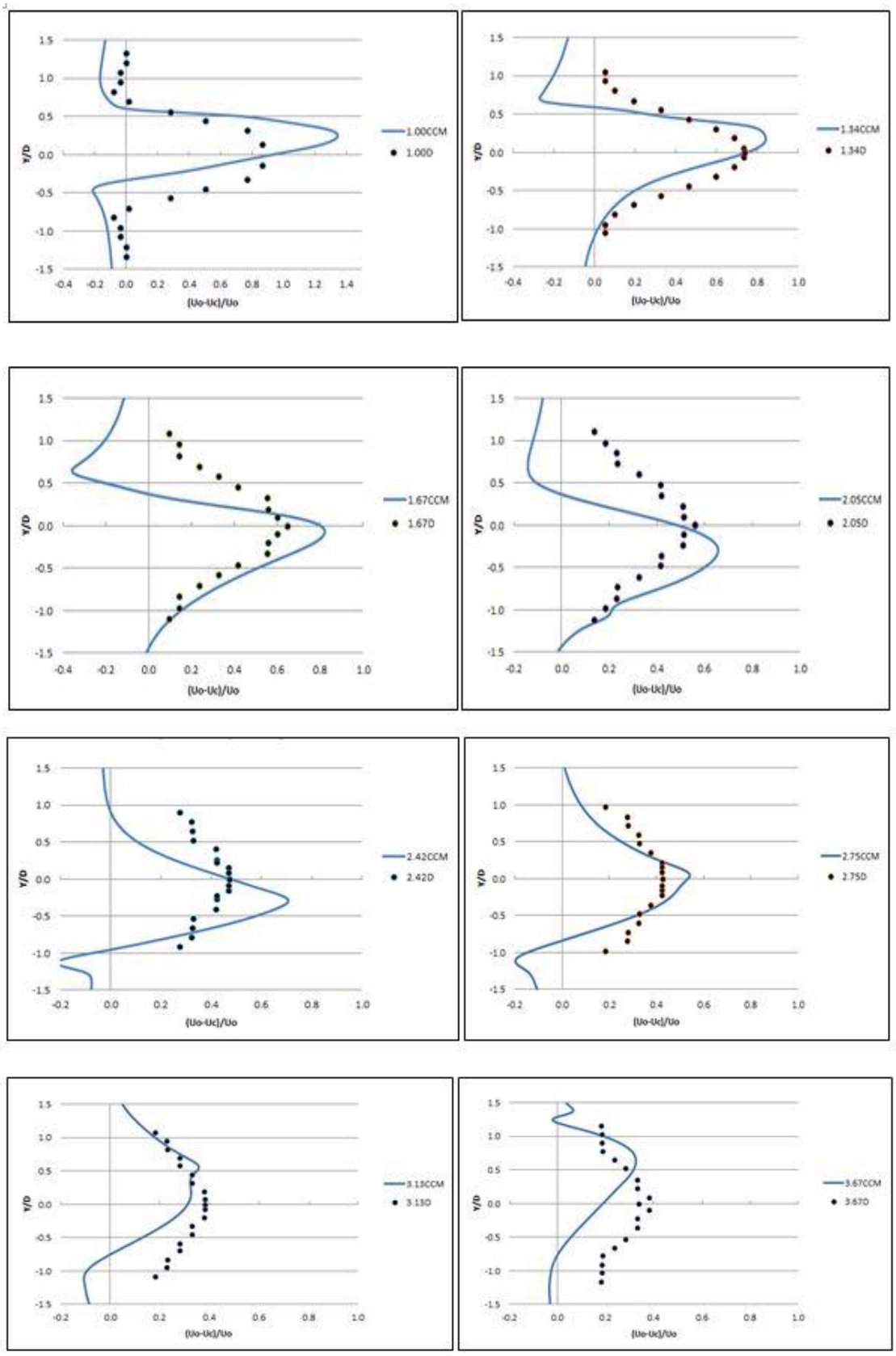

Figure 3-6 Cylinder wake velocity profile prediction

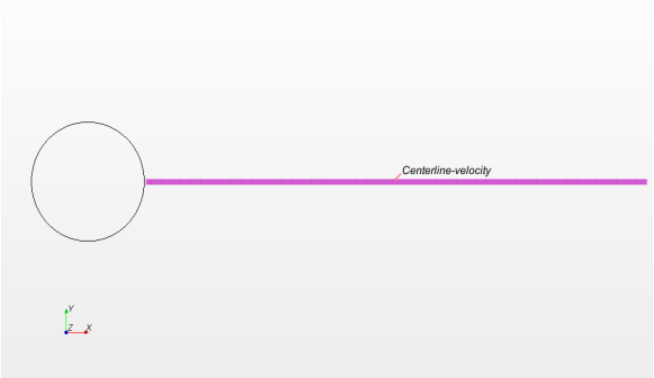

Figure 3-7 Line probes for centreline velocity

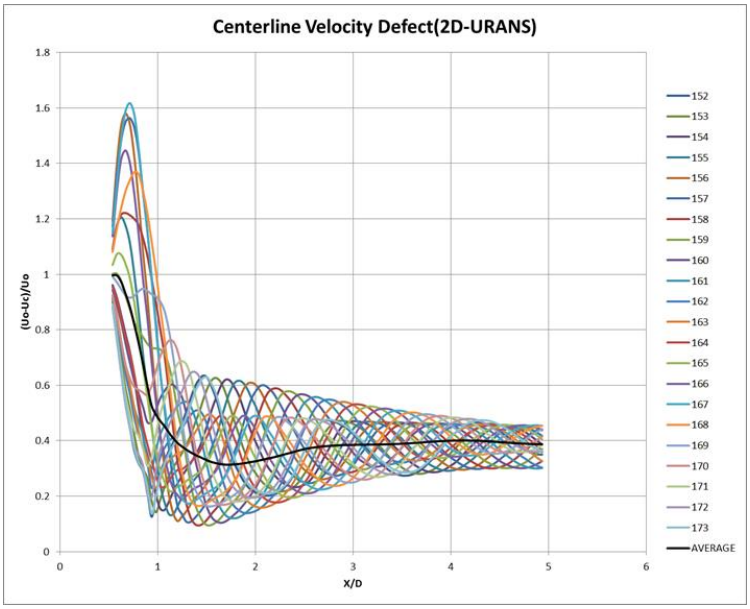

Figure 3-8 Centreline velocity behind the cylinder

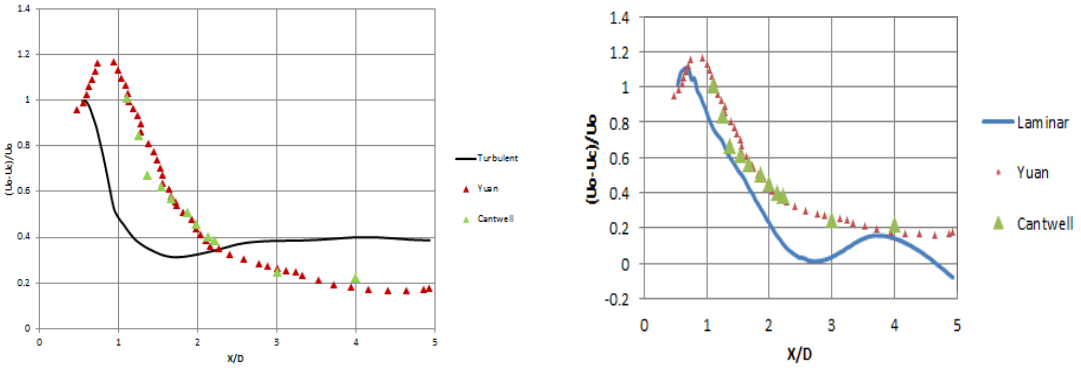

Turbulent solver Laminar solver

Figure 3-9 Centreline velocity comparison

3.3 Airfoil Modelling

3.3.1 Static stall

3.3.1.1 Overview

Most wind turbine rotors consist of streamline sections in the blades, the aerodynamics of airfoil sections has long been a major research topic for the industry. Many series of airfoil are invented from different institutions (NWTC, Delft, DTU, NWIT) and used for HAWT. Sandia VAWT designs adopted the NACA four digit airfoil.

The thickness distribution for the NACA four-digit sections is determined in the following formulation (Abbott and Von Doenhoff, 1959):

$$\pm y_t = \frac{t}{0.20}\left(0.29690\sqrt{x} - 0.12600x - 0.35160x^2 + 0.28430x^3 - 0.10150x^4\right)$$

where t is the maximum thickness as a fraction of the chord, x is the x coordinate, and y_t is the y coordinate.

The leading-edge radius r_t is:

$$r_t = 1.1019t^2$$

For the NACA four digit airfoil. The first integer indicates the maximum value of the mean line ordinate y_c in per cent of the chord, the second integer indicates the distance from the leading edge to the location of the maximum camber in tenths of the chord. The last two integers indicate the section thickness in percent of the chord. NACA4412 wing section has 4% camber at 0.4 of the chord from the leading edge and is 15% thick. It is easy to know that NACA00XX airfoil are symmetry airfoil of different thickness.

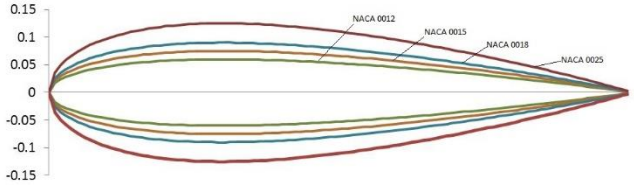

Figure 3-10 NACA00XX airfoil

The aerodynamic performance characteristics of different airfoils are usually expressed by its lift, drag, and moment coefficient in respect to angle of attack, an angle of between the incident wind and the airfoil chord. The lift, drag and moment coefficient are measured in experiments.

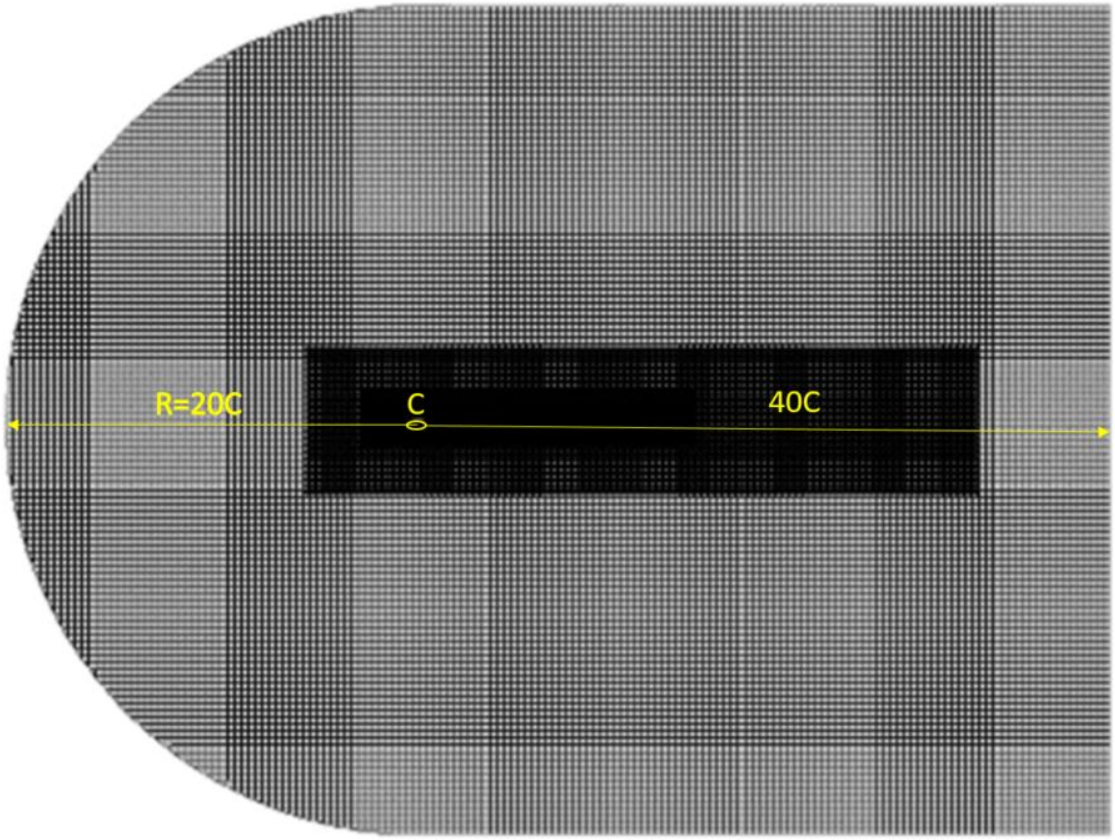

Figure 3-11 2D mesh of NACA 0015 Airfoil

3.3.1.2 Simulation setup

The aerodynamic performance of NACA0015 is studied in 2D simulation. Because the airfoil is used in many lift driven types of VAWT, the lift coefficients of the 2D airfoil at different angles of attack are obtained through CFD simulation and are compared to experimental measurement. Dynamic stall behaviour of the same 2D airfoil is also explored.

The layout of the 2D mesh is shown in Figure 3-11, there are about 60000 cells in the 2D mesh, this is due to the memory limitation of the computer by the time it was computed.

The lift coefficient is measured at a series of attack from 0 degree to 22 degrees at one-degree interval. The airfoil is fixed in the 2D numerical wind tunnel created, with its chord point to the inlet and parallel to the top and bottom boundary. The angle of attack is implemented from the inlet.

This method of controlling angle of attack is more efficient way than changing the airfoil angular position in the wind tunnel, in which 3D mesh has to be recreated each time and converted to 2D mesh, introducing potential geometry errors. The current method is able to ensure that the same mesh is computed throughout for flow with different angles of attack.

The Reynolds number of the for the testing is 2000000, which could be experience by a rotor blade during its normal operation. The experimental dataset used for comparison is called ASTAL from Dr Andrew Shires, the same dataset is used in the Cranfield Wind Turbine Code. The dataset also include performance data of other symmetry airfoils at different Reynolds number.

The inlet speed is 36m/s for the model. Three turbulence models are tested for using the same default turbulence intensity settings of 1%. 60 steady state simulations were completed,

3.3.1.3 Results and discussion

The lift coefficients from simulations are listed below in Table 3-4 and presented in Figure 3-12. The predictions of different models before 14° are very close to each other for the three turbulence models used. The k-ε model predicts a slightly higher stall AOA at 16°, and a higher lift coefficient 1.324.

Table 3-4 Lift coefficient of NACA 0015 airfoil at Re=2000000

AOA(°)	$SST\ k-\omega$	$Realizable\ k-\varepsilon$	$Spalart-Allmaras$	Astal	Maximum Err %
1	0.1097	0.1103	0.1105	0.11	0.45
2	0.2184	0.2198	0.2174	0.22	1.18
3	0.3254	0.3277	0.3280	0.33	1.39
4	0.4313	0.4362	0.4375	0.44	1.98
5	0.5347	0.5381	0.5384	0.55	2.78
6	0.6351	0.6437	0.6291	0.66	4.68
7	0.7287	0.7481	0.7380	0.77	5.36
8	0.8287	0.8509	0.8291	0.88	5.83
9	0.9210	0.9535	0.9257	0.9574	3.80
10	1.0085	1.0116	1.0103	1.0433	3.34
11	1.0893	1.0981	1.0922	1.1138	2.20
12	1.1625	1.1684	1.1608	1.1667	0.51
13	1.2184	1.2191	1.2185	1.1949	2.03
14	1.2552	1.2877	1.2465	1.1962	7.65
15	1.2608	1.3129	1.2473	1.1744	11.79
16	1.1614	1.3247	1.2528	1.1356	16.65
17	1.0234	1.2551	1.0378	1.0921	14.93
18	0.9074	1.1483	0.9456	1.051	13.66
19	0.8350	0.9272	0.8485	1.0173	17.92
20	0.7020	0.8599	0.7838	0.9954	29.48

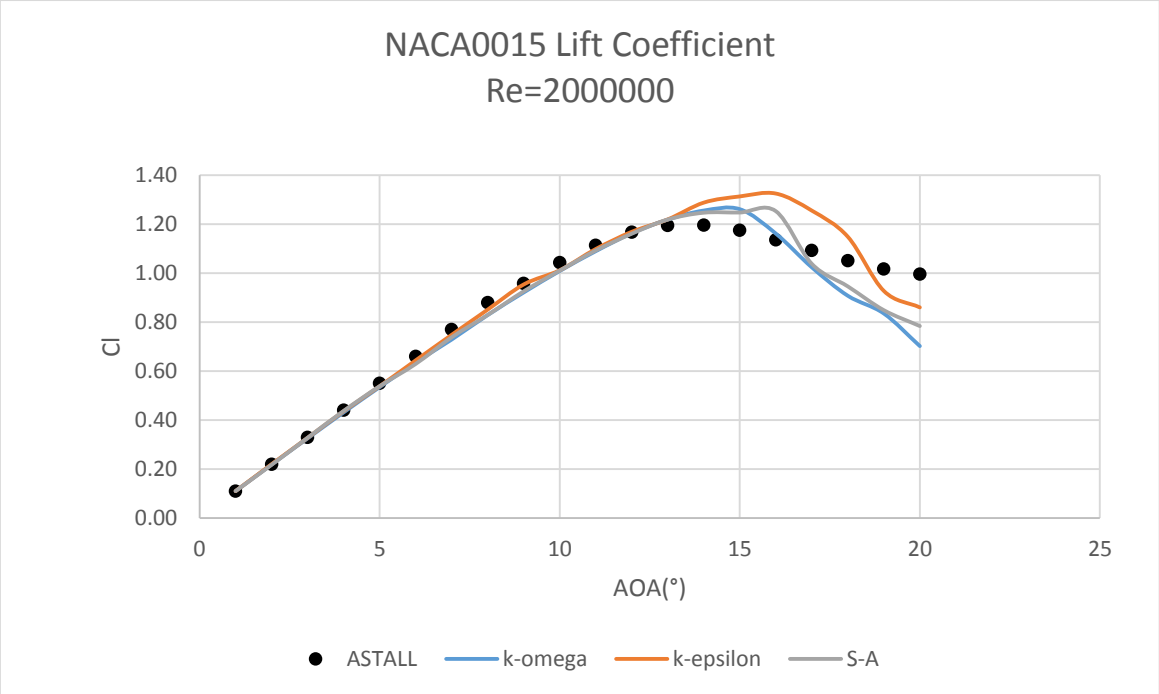

Figure 3-12 Lift coefficient of NACA0015 airfoil of three models

3.3.2 Dynamic stall

3.3.2.1 Overview

When VAWT is rotating, the local angle of attack will change as a function of azimuthal angle θ and tip speed ratio and X and δ, the angle between blade normal and the equatorial plane. According to Paraschivoiu(Paraschivoiu, 2002) the local angle of attack could be written as follows:

$$\alpha = \arcsin\left(\frac{\cos\theta cos\delta}{\sqrt{(X - sin\theta)^2 + cos^2\theta cos^2\delta}}\right)$$

local angle of attack of turbine at two different tip speed ratios are shown below.

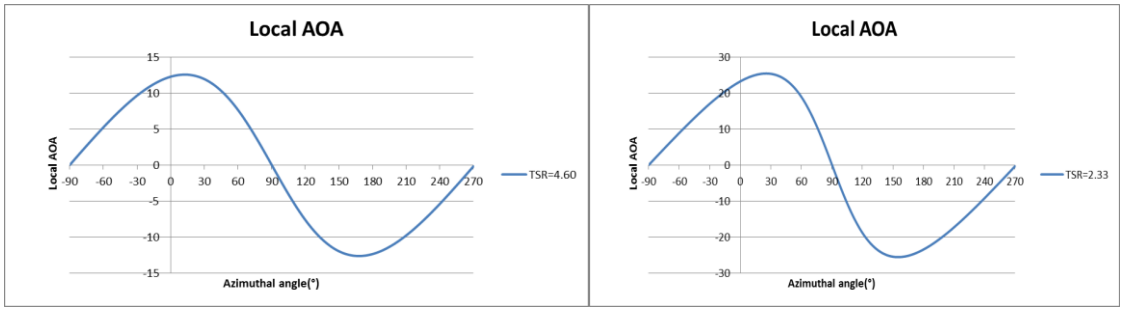

Figure 3-13 Local angle of attack at different tip speed ratios

The rapid change of angle of attack of VAWT make it prone to dynamic stall. Dynamic stall has long been known as an issue affecting VAWT performance, and to model the dynamic stall accurately poses great challenges to researchers. (Ferreira et al., 2007, Hamada et al., 2008, Qin et al., 2011)

But they are carried out based on a different software package. In the presented thesis, STAR-CCM+ is used.

There are three stages of the dynamic stall process: vortex formation in the leading, vortex travelling along the suction side, vortex shedding from the suction side. 2D dynamic stall experiment of NACA0015 airfoil by Rhee (Rhee, 2002)was selected for verification. Three different flow regimes were chosen for modelling as shown in Table 3-5.

Table 3-5 Configuration of dynamic stall cases

Flow regime	α	v	K	ω	Re
No stall	$\alpha = 4° + 4° * sin\omega t$	$29\ m/s$	0.038	$21rpm$	$\sim 2 \times 10^6$
Light stall	$\alpha = 11° + 4° * sin\omega t$	$29\ m/s$	0.095	$52rpm$	$\sim 2 \times 10^6$
Deep stall	$\alpha = 17° + 5° * sin\omega t$	$29\ m/s$	0.095	$52rpm$	$\sim 2 \times 10^6$

α is the angle of attack, v is the inlet wind speed, K is the reduced frequency, ω is the pitching frequency, and Re is the Reynolds number calculated based on a unit chord length.

3.3.2.2 Simulation setup

Since the dynamic stall is a time dependent phenomenon, unsteady simulation adopted instead of steady state simulation as in the case of static stall. However, the same set mesh layout is used as shown in Figure 3-11.

There are many ways to implement motion in STAR-CCM+, including morphing, rigid body motion, and moving reference frame et al.(CD-adapco, 2014). Moving reference frame approach can be only used in steady state simulation. and for rigid body motion approach require a separate region to be made and extra boundary and interface. Therefore, morphing motion was added to the airfoil boundary. For simplicity, the constant part of the angle of attack is implemented by setting the inlet angle.

Table 3-6 Parameters used for defining motion in STAR-CCM+

	Inlet angle	Rotation rate	Time step
No stall	4°	0.1535*cos(2.199*$Time)	0.071s
Light stall	11°	0.4*cos(5.4454*$Time)	0.028s
Deep stall	17°	0.48*cos(5.4454*$Time)	0.028s

The maximum physical time set for the simulation is set to equal 60.0s.

3.3.2.3 Results and discussion

Simulation results are shown in Figure 3-14 to Figure 3-16. No stall and light stall case, results from realizable $k-\varepsilon$ model is shown blow; for the deep stall case. comparison is made throughout the three turbulence models.

It is shown that the realizable k-ε model has given relatively good prediction at no stall and light stall flow regimes.

As for the deep stall case, all three turbulence models underestimate the lift coefficient, Spalart-Allmaras models has given slight better prediction. A possible explanation for this may be referred to results of Section 3.3.1, as the three turbulence models fail to predict the lift coefficient accurately when the angle of attack is over 14°, while the angle of attack for the deep stall case is 12° to 22°.

Velocity contour is shown in Figure 3-17 for one complete period for all three turbulence models. It can be observed that as the airfoil is pitching up during which the angle of attack increases. A low velocity zone is formed on the upper surface of the airfoil. This low velocity zone grows as the airfoil is pitching down, during which the angle of attack decreases. The velocity zone become smaller as the angle of attack increase again. The influence of the turbulence model is not noticeable as similar pattern is observed across the three different turbulence models.

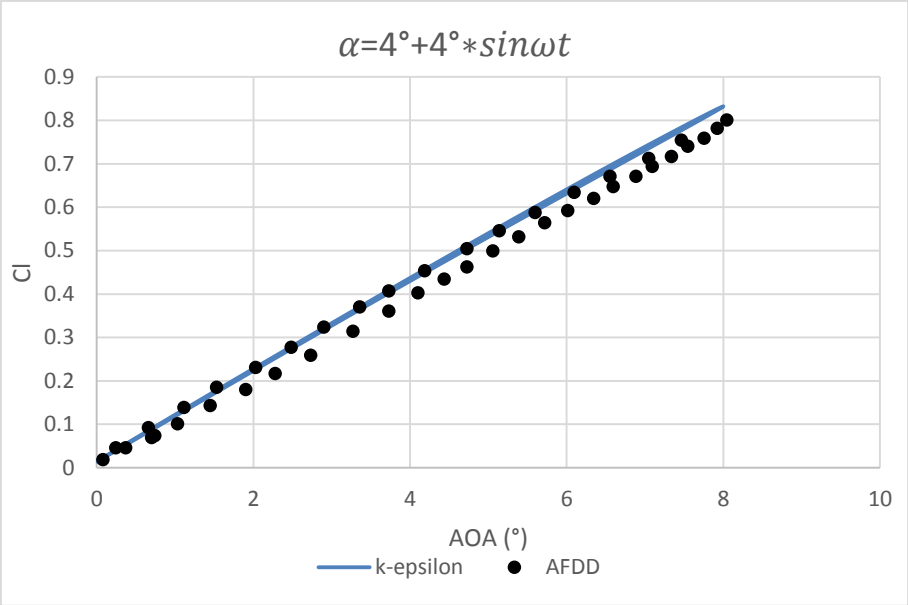

Figure 3-14 Lift coefficient prediction of NACA0015 airfoil at α=4°+4°$*sin\omega t$

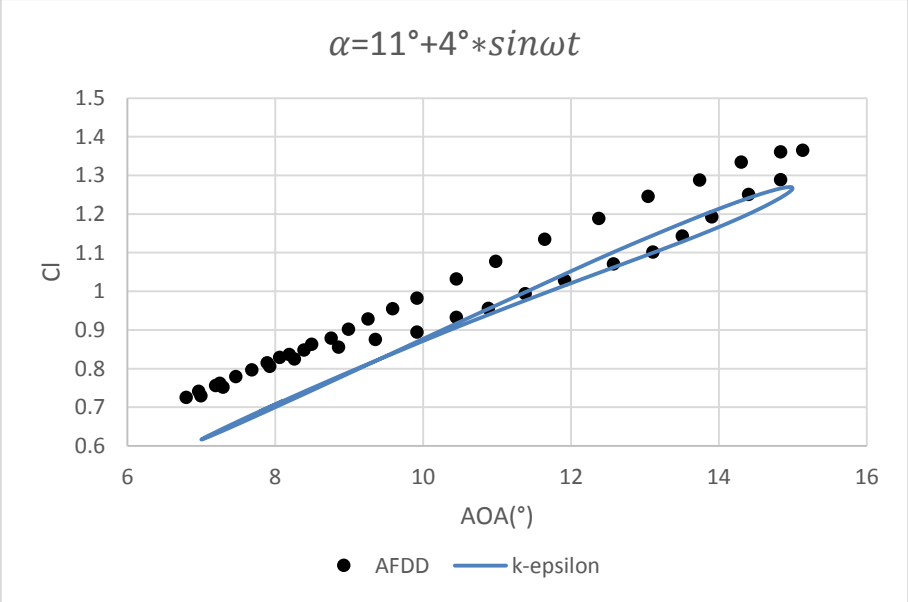

Figure 3-15 Lift coefficient prediction of NACA0015 airfoil at α=11°+4°$*sin\omega t$

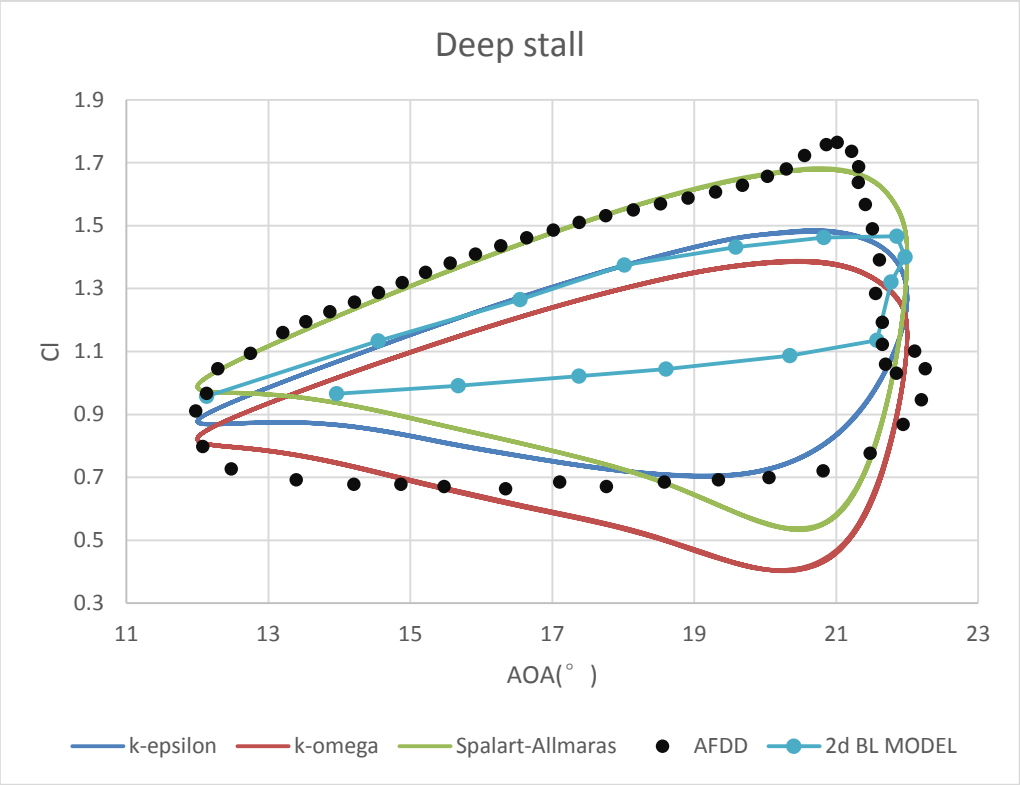

Figure 3-16 Lift coefficient prediction of NACA0015 airfoil at α=17°+5°$*sin\omega t$

$Realizable\ k-\varepsilon$	$SST\ k-\omega$	$Spalart-Allmaras$
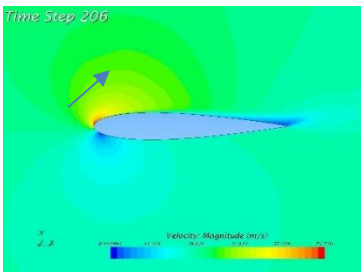	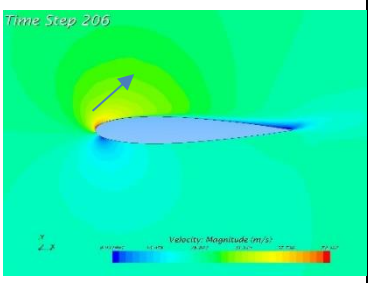	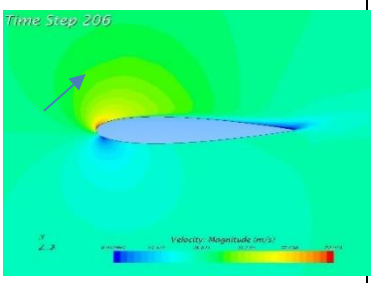
206 time step	206 time step	206 time step
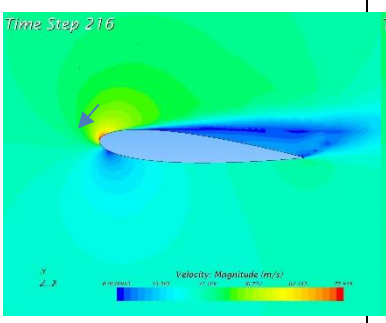	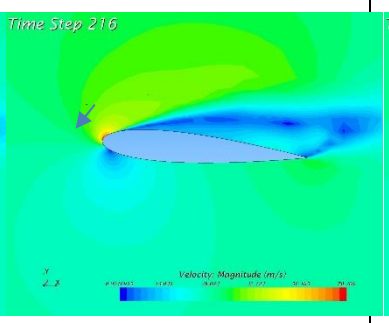	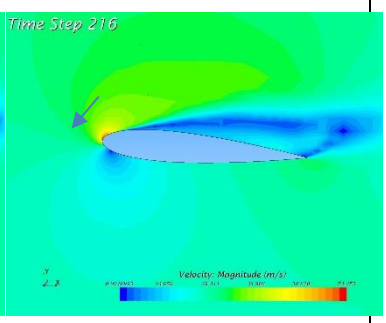
216 time step	216 time step	216 time step

$Realizable\ k-\varepsilon$	$SST\ k-\omega$	$Spalart-Allmaras$
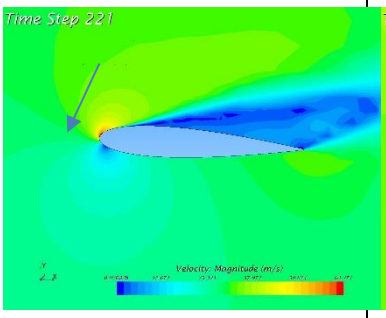	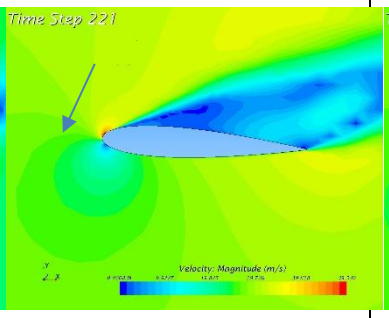	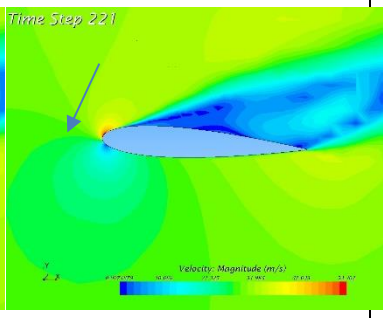
221 time step	221 time step	221 time step
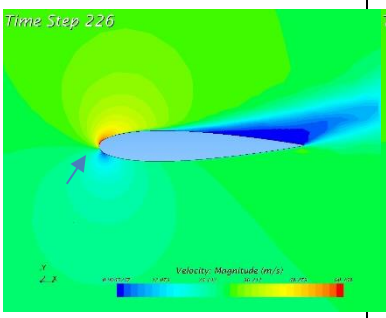	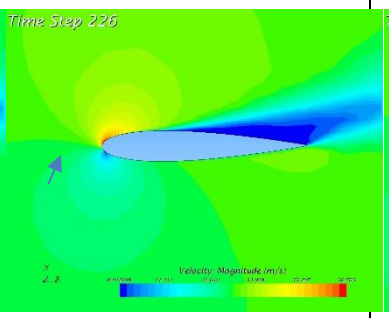	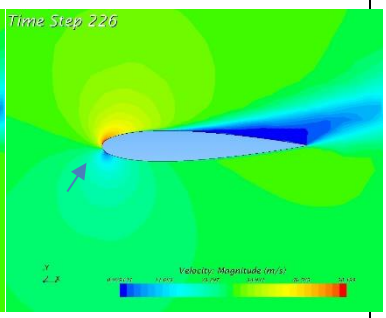
226 time step	226 time step	226 time step

Figure 3-17 Velocity contour of NACA0015 at deep stall

3.4 Rotating VAWT Modelling

3.4.1 Overview

An accurate near wake modelling is the foundation of far wake modelling. as it gives the onset of the far wake simulation. On the other hand, the near wake is closely linked to aerodynamic performance of VAWT, an accurate near wake modelling could provide more insight for the VAWT design optimisation.

A number of simulations of VAWT were carried out on ANSYS FLUENT(Simão Ferreira et al., 2007, Qin et al., 2011), a simulation using STAR-CCM+ could be a valuable alternative for validation purposes.

2-bladed SNL-17m VAWT was selected for the simulation. The chord of the blade is 0.615m, and has a NACA0015 airfoil, the rotor speed is 38.7rpm, the original test was reported by Akins(Akins, 1989).

Performance of the wind turbine Several tip-speed ratios were tested in the original experiment using pressure tap installed at the equatorial blade section. Performance at tip-speed ratios=2.3 and tip speed ratio=4.6 were chosen by Allet (Allet and Paraschivoiu, 1995)to evaluate the DMST model and Vortex model. The objective of the simulation is to setup model and obtain time-accurate blade force and compare with the experiment and other engineering models.

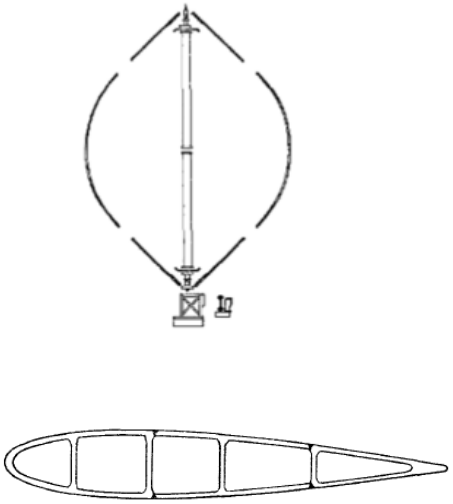

Figure 3-18 Configuration of SNL 17m VAWT

(source: SAND80-0984)

Table 3-7 Key Parameter of 2D simulation

Turbine Height	25.1m
Rotor Diameter	16.7m
Blade chord	0.615m
Airfoil section	NACA0015
Tower diameter	0.762m
Rotor speed	38.7rpm (selected for comparison)
Tip speed ratio	4.6 / 2.33 (selected for comparison)

(source: SAND80-0984, (Akins, 1989), Allet(Allet and Paraschivoiu, 1995))

3.4.2 Simulation setup

Mesh over the equatorial section of the VAWT was created using trimmed mesh in 3D and converted to 2D, the total cell 2D count is around 500,000. The trimmed mesh is used because the relative mild requirement in the RAM compared to the Polyhedral mesh, using trimmed mesh could allow one to produce a larger domain.

The flow domain consists of a rotating inner region and a fixed fluid region. The rotating cylinder region is 1.2D in diameter, and the fixed fluid region is 10D wide and 5D to the inlet and 10D to the outlet.

Velocity inlet is assigned to the inlet, the pressure outlet is assigned to the outlet, wall boundary is assigned to blades and tower, all other boundaries are treated as symmetry boundaries.

Mesh alignment was enabled to improve the mesh quality. in the 3D mesh stage, mesh quality was checked to ensure no negative volume cell existed.

Per-region mesh is used because the trimmed mesher could not operate in multiple regions. One shortcoming of this approach is the mesh conformity will be compromised is the two regions have different mesh size. the boundary between rotor region and fluid region are customized to mesh in the same size and the prism layer at this boundary is disabled to improve the transition of fluid. Base size of the mesh is set to be equal the chord length 0.61, and the local refinement region were added to blade and tower where high velocity gradients are expected.

Different from the dynamics stall airfoil case, the motion was added to the rotor region as a rigid body motion. This is a better approach than the morphing because a full cycle of the rotor will significantly change the mesh quality during the simulation using morphing and cause divergence in the simulation. An alternative to simulate the motion is to use a moving reference frame(MRF), in which the mesh does not move, the motion is added through a source term in the governing equation. But in STAR-CCM+, MRF is restricted in steady flow

solution, so it is not suitable for the comparison of variation of force coefficients where a time-accurate solution is required.

Because of the rigid body motion, the two regions are still likely to interfere one another during the simulation. To verify the mesh, a full revolution is simulated to ensure there is no interfering points.

Time step is selected to enable the time marching of solution. To capture the variation, general time step was chosen according to the rotor speed. the period of the rotor is 60/38.7=1.55s. Therefore, to reach an accuracy of 1°/time step, the time step has to be 1.55/360=0.004305s. Total simulation time was chosen as 60 s.

It is necessary to have adequate iterations to ensure the solution is fully converged within each time step. By default, the inner iteration for 15, but it was proved from an initial run to reach a converged solution with the targeted residuals lower than 10^{-4}. So, the default inner iteration was removed and new stopping criteria of the inner iteration number were created. The new stopping criteria were based on the residual values including continuity, x momentum and y momentum, and turbulent kinetic energy, only when all the residual values lower than the required residual value 10^{-6}, can the simulation proceeded to the next time step. It was later discovered in a verify simulation that at certain time step, the minimum residual could obtain is approximate 10^{-5} and the simulation could not step up to next time step. An extra criterion to force the simulation continue is introduced. It is based on the observation that at about 100 iterations the residuals of a time step could all stay at 10^{-5} or lower, therefore, an inner iteration number maximum is set to 100 in addition to the previous stopping criteria set based on the residual values lower than 10^{-6}. It is a trade-off of accuracy and efficiency.

The lift and drag coefficient reports are created on one blade before the simulation to extract the data, the reference velocity is set to match the inlet velocity, the reference area is set to match the chord length because it is in 2D.

By changing the inlet speed, force predictions of two tip speed ratios are investigated.

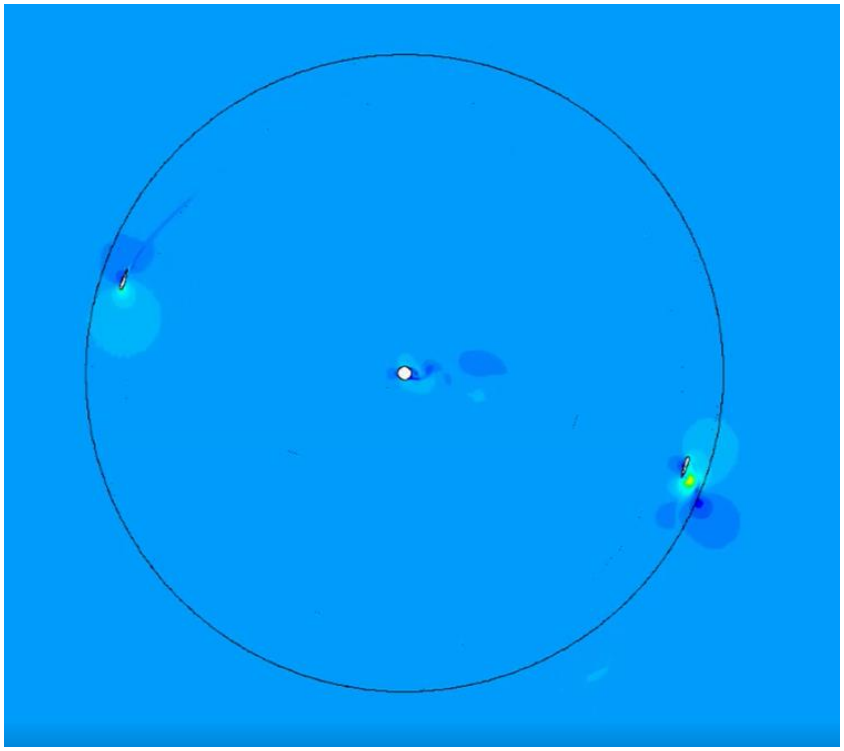

Figure 3-19 velocity contour of SNL-17m VAWT TSR=4.6

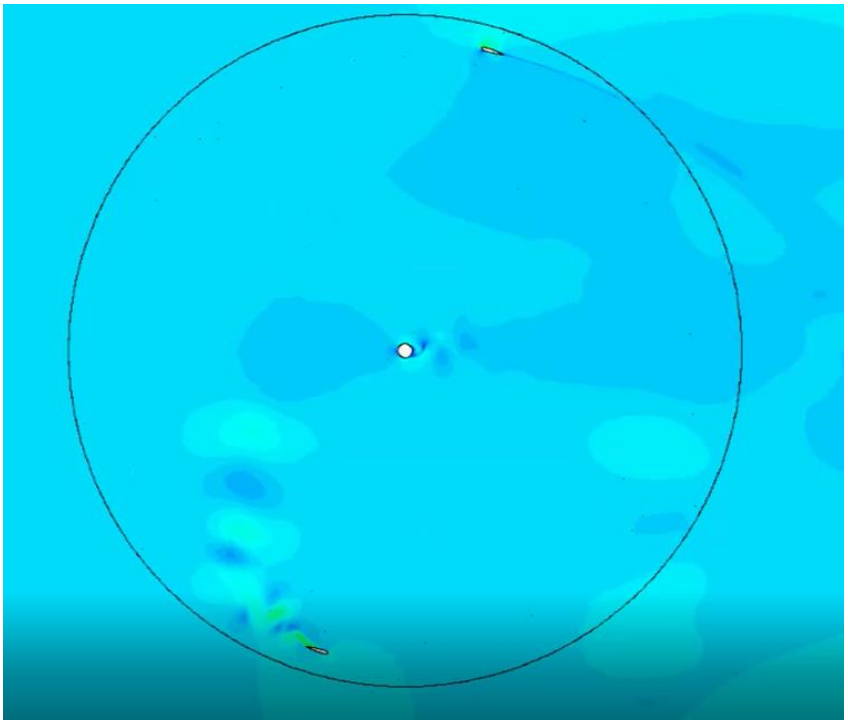

Figure 3-20 Velocity contour of SNL-17m VAWT TSR=2.33

3.4.3 Results and discussion

Results from simulation using a SST k-ω model is included below. SST k-ω model is selected because it has very good behaviour in adverse pressure gradients and separating flow. It was successfully applied to the modelling of a pitching airfoil by Gharali et al(Gharali and Johnson, 2012)

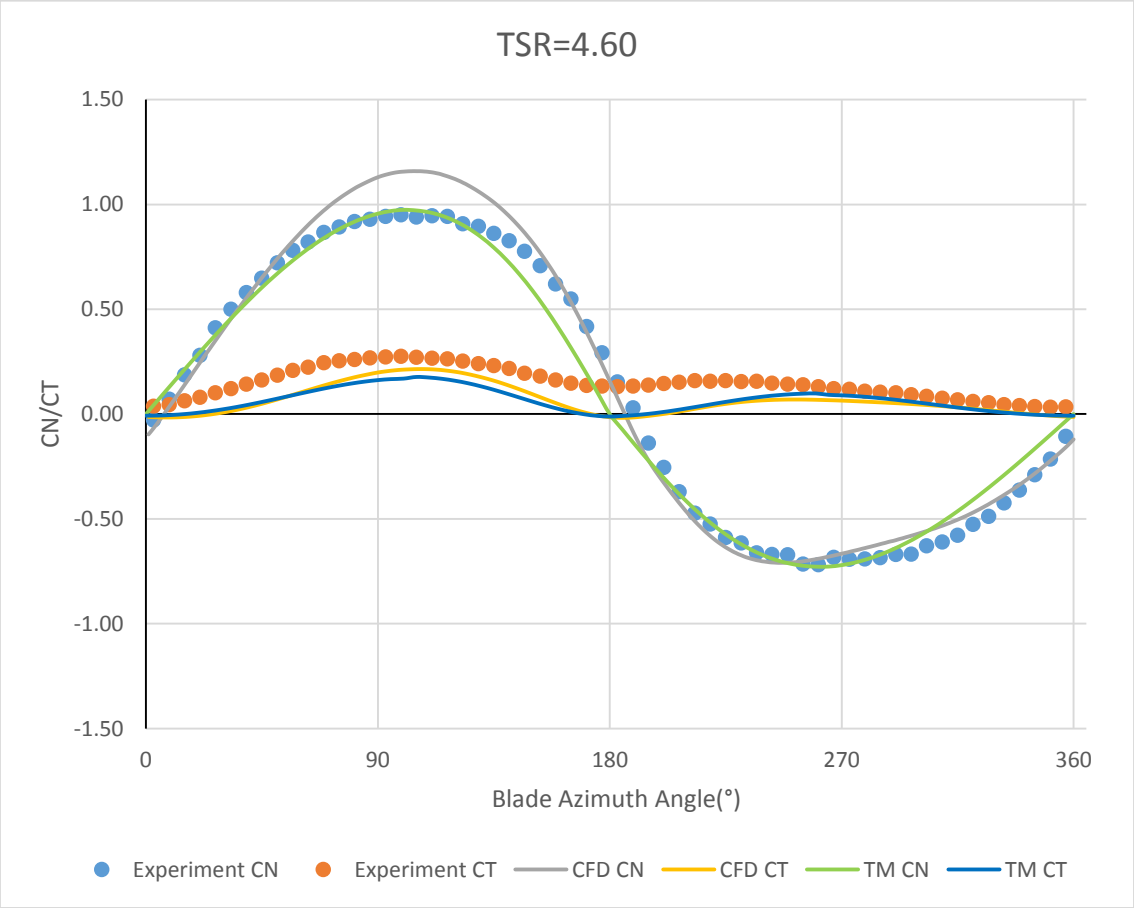

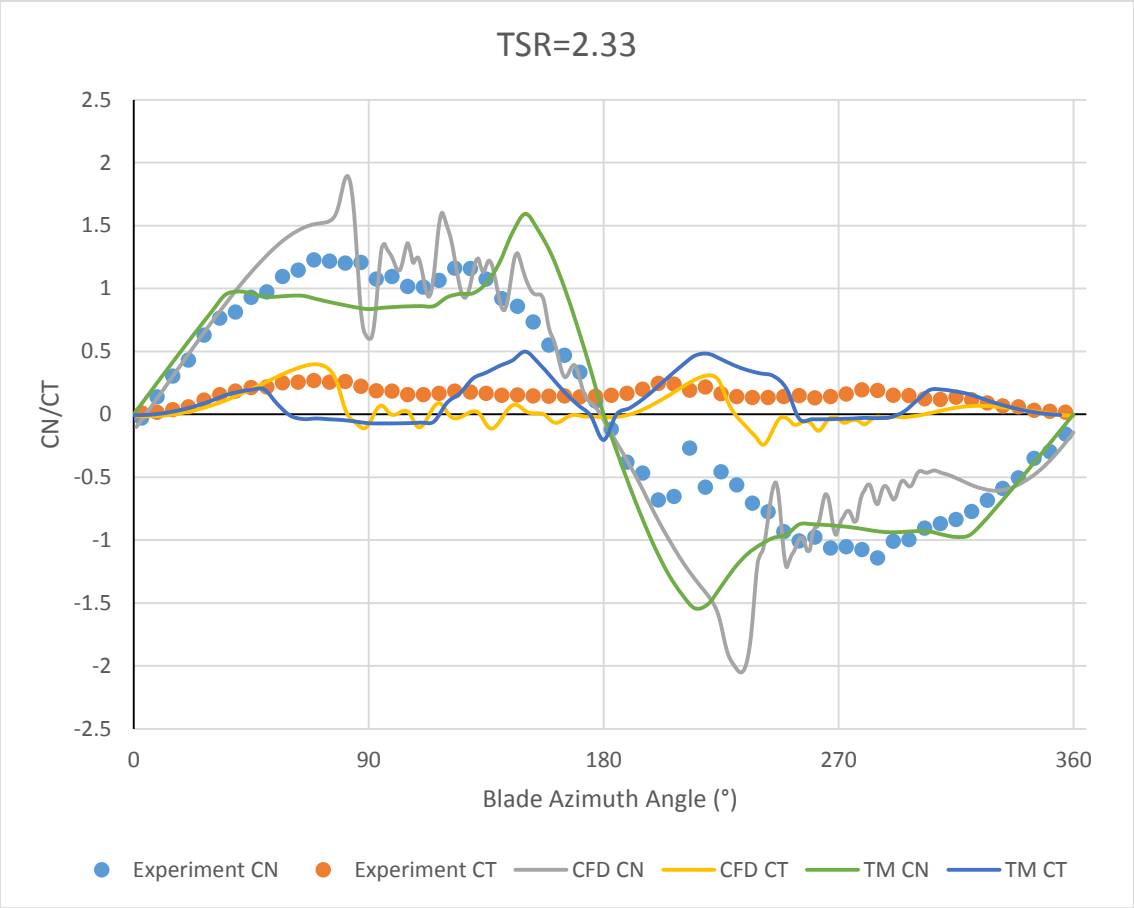

Figure 3-21 Normal and tangential force coefficient of VAWT

The above figures depict the results of normal and tangential force coefficients of one blade derived from the extracted lift and drag coefficient. For the low wind speed case(TSR=4.6), the normal force and tangent force are in good agreement with the measurement. 10% over prediction occurs at $\theta = 90°$ for the normal force, this might due to the high angle of attack at the upwind cycle. the tangent force predicted by the model is very close to the measurement, but model under predicts the tangential force.

As for the high wind speed case (TSR=2.33), both tangential force and normal force fluctuates significantly, indicating possible flow separation and dynamic stall. While the CFD model can capture the characteristics, the normal force predicted for the downwind side (180° to 360°) is much larger than the measurement, and a noticeable spike can be found. It corresponds to the downward cycle of a pitching airfoil under large angle of attack, where large vortex sheds from the

lower pressure sides, and dynamic stall happens. But similarly, the tangential force is under predicted.

3.5 Summary

In this chapter, some classic cases closely associated with the performance of a VAWT is simulated using RANS method on STAR-CCM+. The aerodynamic performance of VAWT is determined through CFD modelling based on STAR-CCM+.

For Re=140000, circular cylinder wake simulation based on RANS yields better results when laminar model is used. The vortex formation process is well captured.

As for the airfoil simulation, both static stall and dynamic stall are simulated. Three turbulence closure models are used for the static stall case to study the angle of attack range from 0° to 20°, the results show very good agreement at angle of attack less than 16°, at high angle of attack the prediction accuracy decrease greatly, about 20 percent error could be expected at 20-degree angle of attack.

The dynamic stall of airfoil is modelled using the morphing mesh technology of STAR-CCM+, the motion is implemented by a rotation rate. The tested turbulence models tend to underestimated the lift coefficient. One equation Spalart-Allmaras model provide the best prediction at deep stall case.

The simulation of a VAWT is carried out in 2D based on STAR-CCM+, the two regions are created in trimmed mesh to simulate a time-dependent behaviour of VAWT. The motion of the VAWT is implemented using rigid body motion. Two different tip-speed ratios are studied. The prediction of the high tip-speed ratio is in good agreement with other model and experiment. The predicted maximum normal force coefficient is 10% higher than the experiment data. As for the low tips-speed ratio case, significant fluctuation is predicted by both the CFD model and a BEM model.

4 FAR WAKE MODELLING

4.1 Introduction

The objective of the far wake modelling is to determine the wake velocity distribution for VAWT and VAWT array. Different approach in modelling far wake for HAWT is reviewed in Section 2.2.

The rotor is typically simplified as actuator disc, or actuator line in the case of HAWT. However, applying these techniques to simplify the rotor of VAWT is beyond the scope the current thesis. Instead, some modelling issues regarding modelling far wake on STAR-CCM+ will be highlighted, a porous disk model from NTUA was selected to study the parameter of turbulence modelling on STAR-CCM+.

Full rotor simulation of far wake is performed on single VAWT and VAWT array to study the wake velocity distribution and wake interaction.

4.2 Porous Disk Modelling

4.2.1 Overview

The objective of the simulation is to understand the wake effects and its cause. Previous results showed underestimation of the near wake velocity deficit. It is believed that this underestimation can be corrected by the presence of a higher turbulence dissipation rate (meaning lower turbulence length scale).

4.2.2 Simulation setup

The wind tunnel experiment for the simulated case was carried out in the wind tunnel of NTUA. The testing area had placed a non-rotating plastic perforated disk of 8mm thick with 200mm diameter. The thrust coefficient is 0.8. free-stream velocity is 10m/s and the turbulence intensity is 10%.

In order to assess the turbulence parameters' influence on the far wake simulation on STAR-CCM+, a parametric study is carried out and list in Table 4-1. The geometry of the case can be found in Rados (2009)

Standard k-ε turbulence model is used in the steady state simulation. Turbulence length scale is compared case 2 and case 3 case 6 case 8. Turbulence intensity is compared in case 1 and case 8. Solver constant is compared case 2 case 4 and cases7.

Table 4-1 Test cases for the porous disk

	L	TI	Cε1,	Cε2	Cμ	σk	σε
case1(default)	0	0.01	1.44	1.9	0.09	1	1.3
case2	D	0.1	1.44	1.9	0.09	1	1.3
case3	5D	0.1	1.44	1.9	0.09	1	1.3
case4	D	0.1	1.12	1.83	0.033	1	1.3
case5	5D	0.1	1.12	1.83	0.033	1	1.3
case6	0.2D	0.1	1.44	1.9	0.09	1	1.3
case7	D	0.1	1.76	1.97	0.09	1	1.3
case8	0	0.1	1.44	1.9	0.09	1	1.3

4.2.3 Results and discussion

Velocity contour is shown in Figure 4-1. Wake profile comparisons are made and the results are depicted in Figure 4-2 to Figure 4-4.

Wake profile comparison based on different turbulence length scale shows a similar trend as stated by the other author, and a smaller turbulence length scale can improve the wake profile prediction.

Wake profile comparison based on different turbulence intensities implies that the turbulence intensities may not be as significant a factor as expected, since no change is observed in the given cases when other parameters being equal.

The default solver parameters give the best predictions in the wake in the three cases compared. A larger constant value of these parameters show no significant improvement in the wake prediction, despite a smaller constant value gives the worst wake prediction among the three cases.

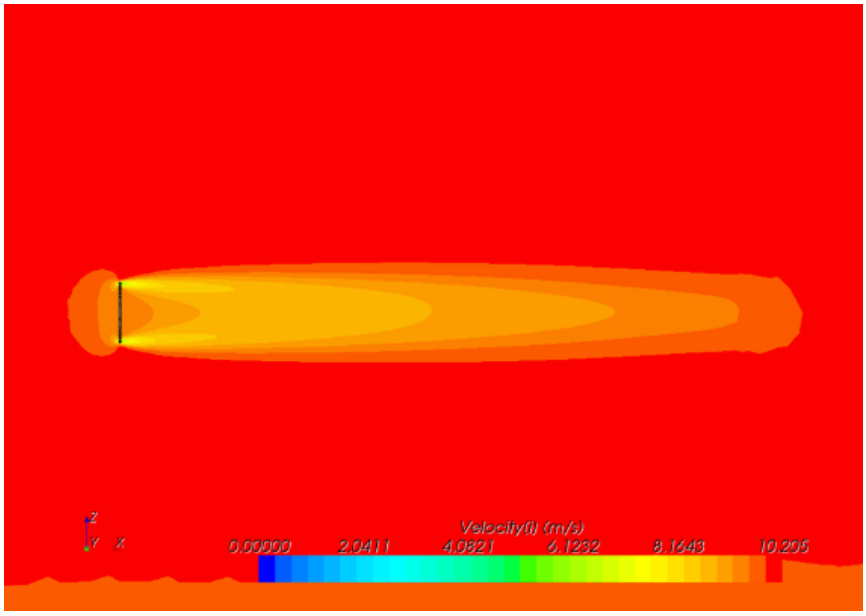

Figure 4-1 Velocity contour of flow around porous disk

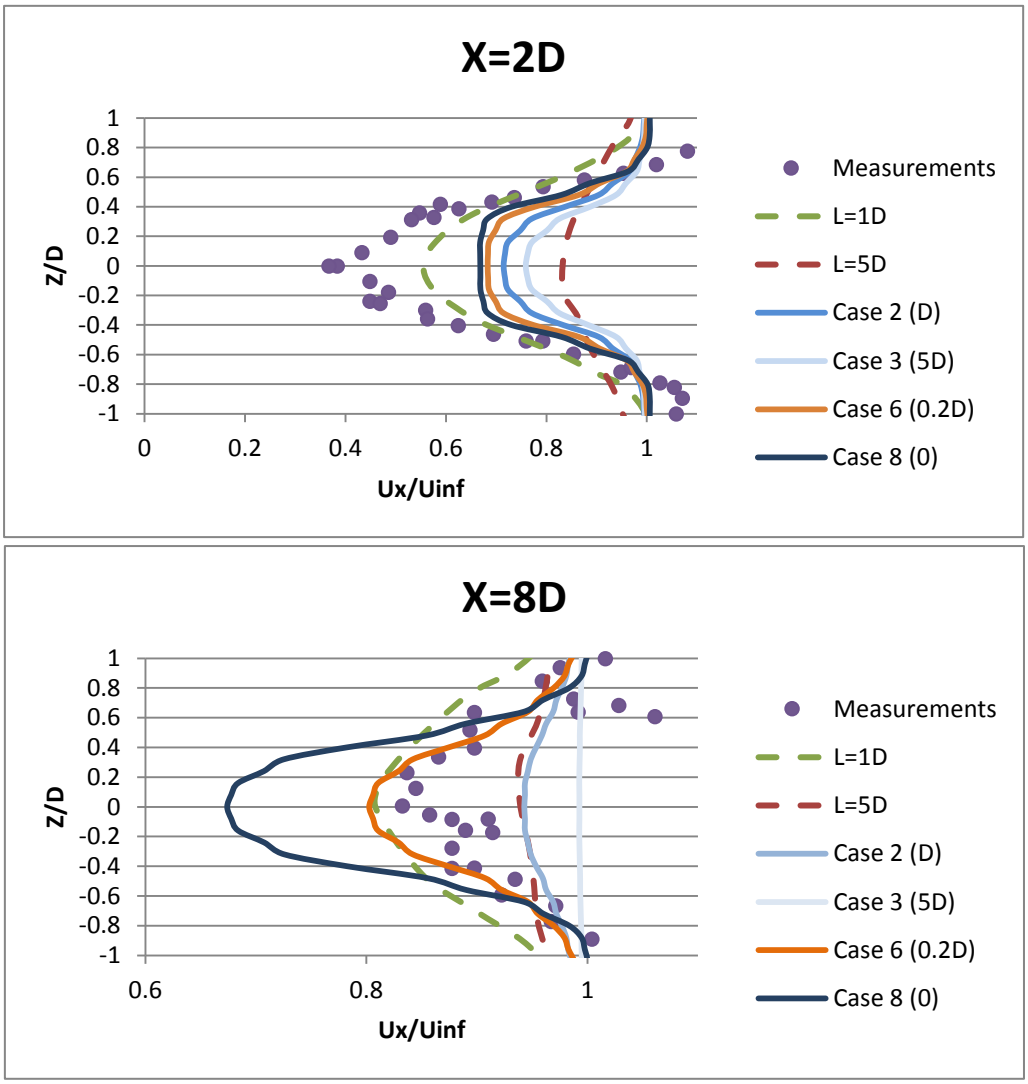

Figure 4-2 Turbulence length scale impact

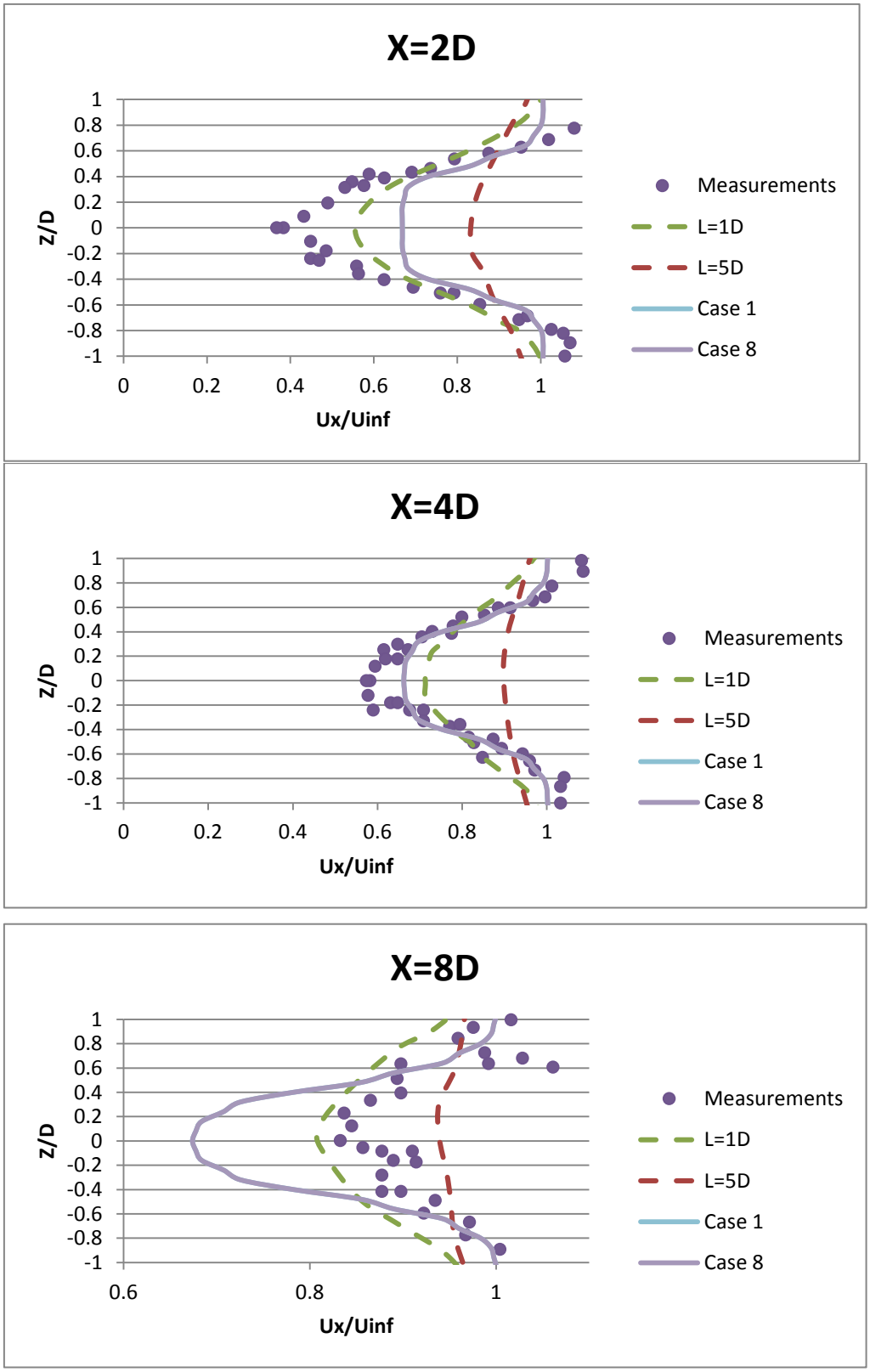

Figure 4-3 Turbulence intensity impact

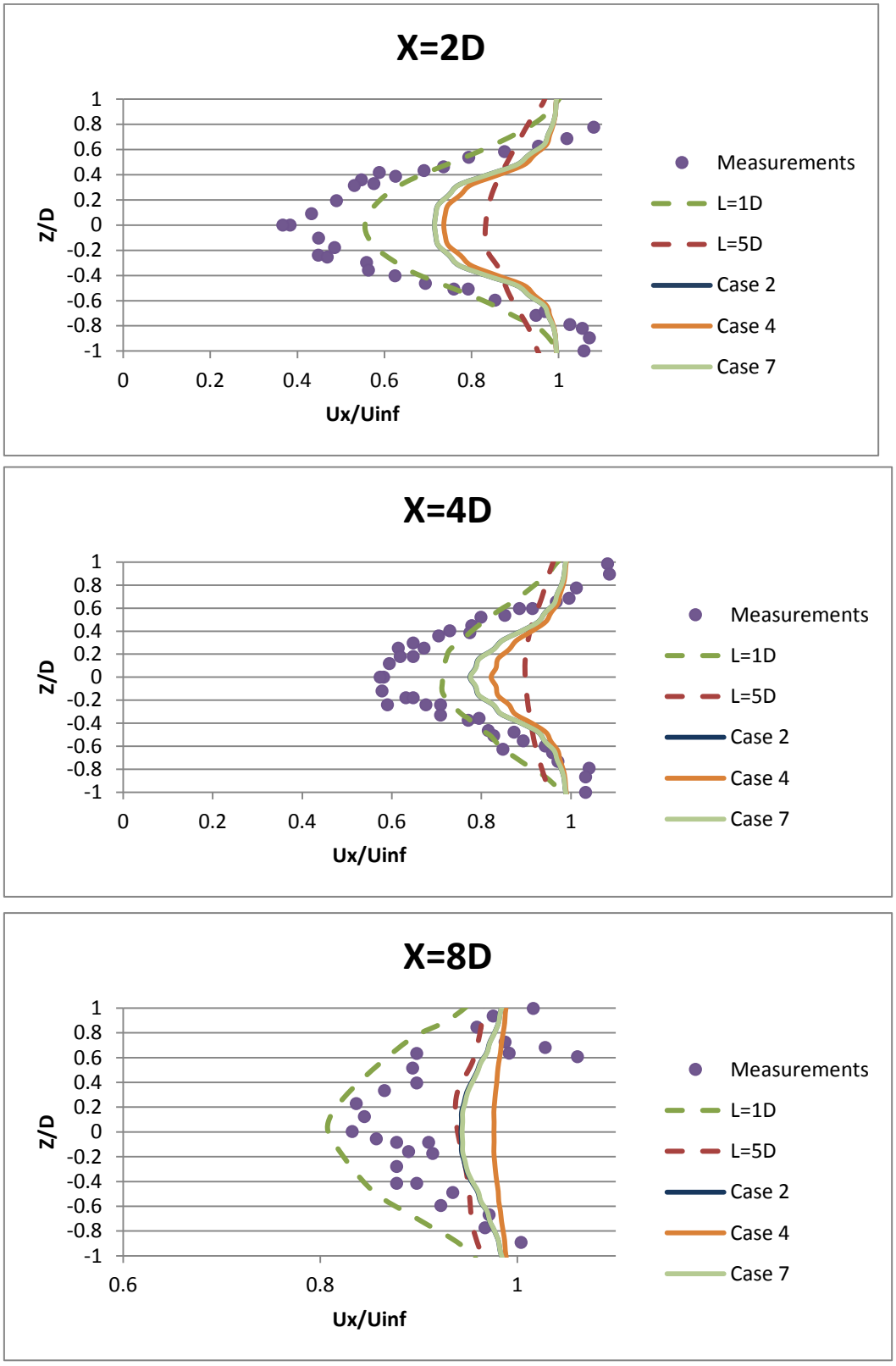

Figure 4-4 Solver constants change

4.3 2D Full Rotor Modelling of Single VAWT

4.3.1 Overview

The objective of the simulation is to model the far wake of single VAWT and determine the velocity under two different conditions. CFD modelling is performed to study the far wake of VAWT based on full-rotor configuration.

4.3.2 Simulation setup

A cone shape refinement region was added based on the mesh used for force prediction of VAWT, this leads to 2D mesh count close to 900,000. Implicit unsteady segregate solver is used, as the same of the previous case. The time step is set to 0.155s (36°/time step) to reduce the solution time. SST k-ω turbulence model is used

The mesh is refined downstream until 3 diameters using a cone shape see below refinement region. This is to improve the mesh resolution. The rotor speed is kept as the 38.7rpm as the previous near wake study.

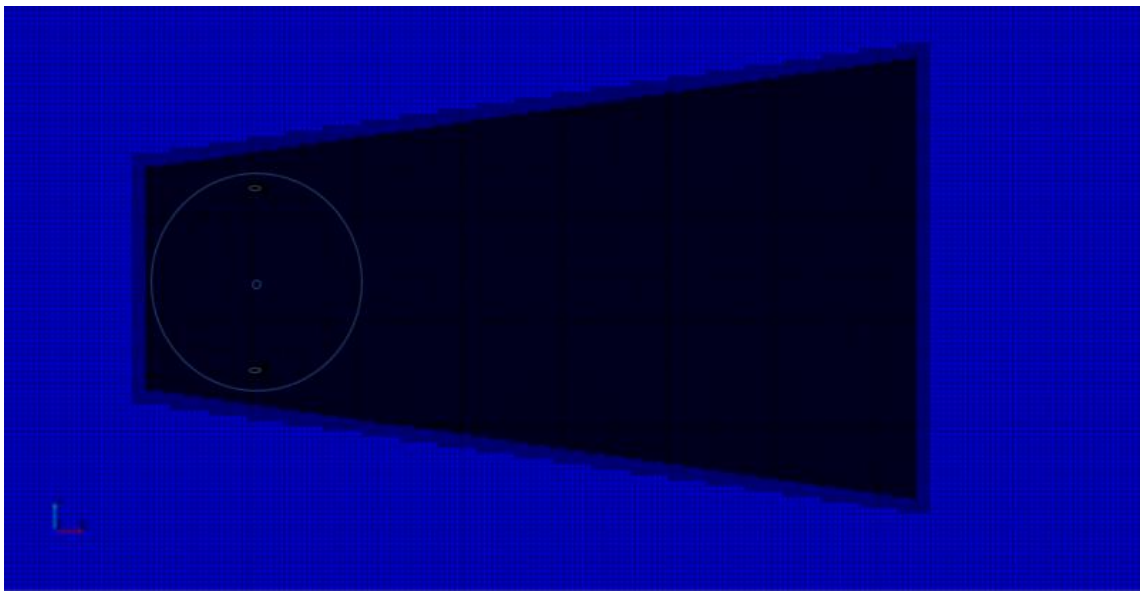

Figure 4-5 Schematic of 2D far wake modelling of SNL-17m VAWT

4.3.3 Results and discussion

Simulation results are shown in shown in Figure 4-6 and Figure 4-7. The far wake profile at two different tip speed ratios of vertical-axis wind turbine is studied.

Clear wake zones can be seen from both tip speed ratios studied. A long and persistent wake is observed at high tip speed ratio case, and a shorter wake region is seen at the low tip speed ratio case.

The velocity deficit of the flow is much larger than the aerodynamics modelling after the introduce of cone refinement region. This might be due to the interface between the fluid and rotor domain, as the 2D mesh generated from the refined 3D mesh is different from previous study.

It is shown that this type of simulation is sensitive to the mesh comformaty and interface quality. Further investigation is required on the mesh quality.

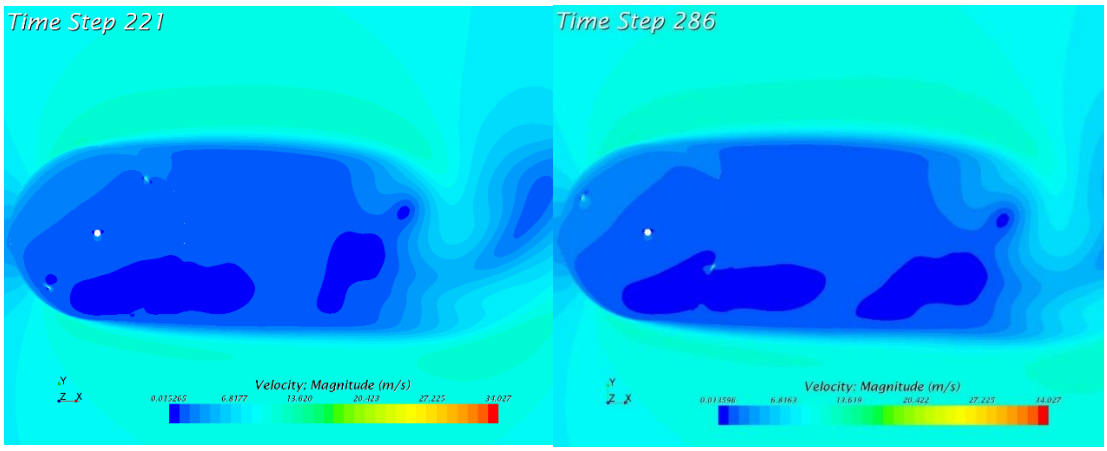

Figure 4-6 Far wake modelling of single VAWT in 2D(λ=2.33)

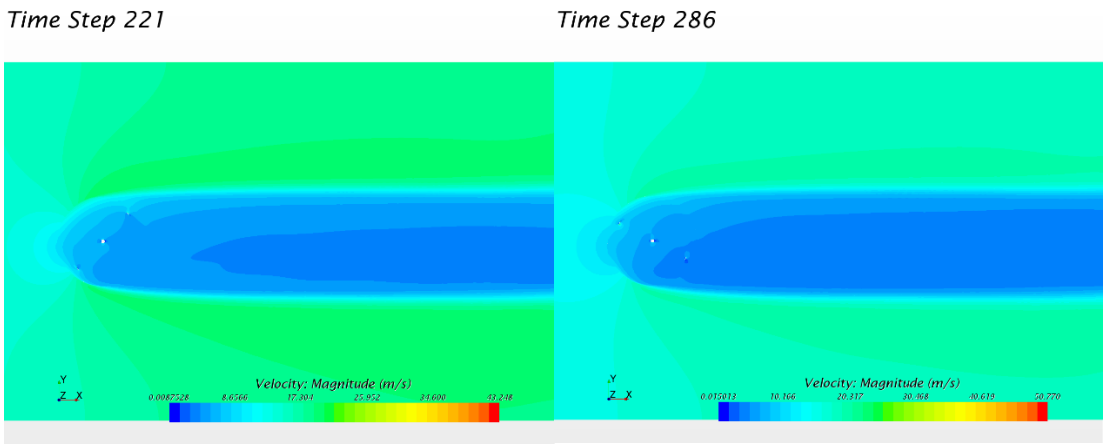

Figure 4-7 Far wake modelling of single VAWT in 2D(λ=4.6)

4.4 2D Full Rotor Modelling of VAWT Array

4.4.1 Overview

The objective of the section is to model the wake interaction of VAWT array and determine the wake influence on turbine performance. A two-turbine array is created to investigate the wake interaction. Two rotating regions and one fixed fluid region are created in 2D.

Based on the far wake modelling of single VAWT, and to avoid the conformity issue of the trimmed mesh and improve the interface quality, the VAWT array mesh is created using polyhedral mesh.

4.4.2 Simulation setup

The flow domain is 160m long, and 80m wide. Because it is generally assumed that wake will dissipate within 3-5 rotor diameters, the flow domain is deemed to be adequate for the wake to develop fully to form self-similar Gaussian profile, and for mitigating the blockage effects, despite Slender domain was applied on LES by Shamsoddin et al(Shamsoddin and Porté-Agel, 2014). The base size of the mesh is 1m, and the prism layer near the wall is set to match the turbine simulated in Section 3.4. The total cell count is about 450000.

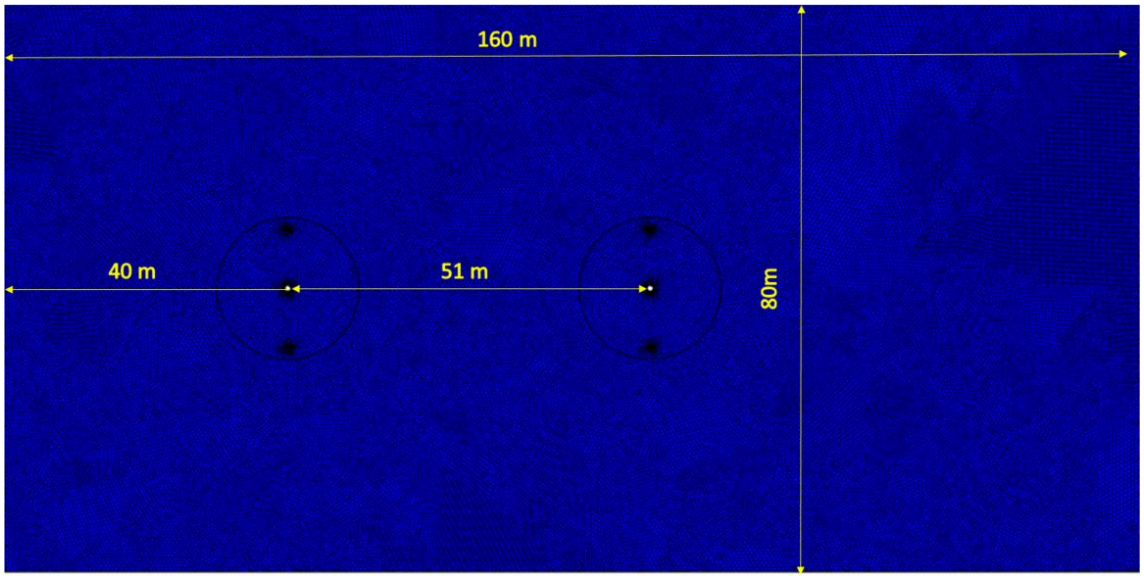

Figure 4-8 Far wake modelling configuration of SNL 17m VAWT array

Two identical VAWT 17m rotors are simulated in 2D. The two rotors are 3 diameters apart and rotating counter-clockwise in the same pace (tip-speed ratio=4.6). The time step is 0.0775s (18°/time step).

4.4.3 Results and discussion

Velocity contour of the simulation are shown below in Figure 4-9. An asymmetric wake is observed across three different turbulence models tested. The flow in the advancing side is slower. Velocity superposition is observed in the wake of the downstream VAWT. Wake asymmetry observed from the velocity contour this agrees with some early field and wind tunnel measurements, such as Liu et al (Liu et al., 1987) and Bergeles (Bergeles et al., 1991)

Force coefficients from the two trubines are compared to assess the performance of the two turbines.

The force coefficients history of upwind VAWT and downwind VAWT are given in Figure 4-10 and Figure 4-11. Little difference is observed across the turbulence models.

Performance impact due to wake effects is depicted in Figure 4-12 to Figure 4-14. The maximum force coefficient predictions by all three different turbulence models are similar to one another. 25% reduction in the force coefficient is observed for the downwind VAW, indicating a potential structural and performance significant of wake effects to VAWT.

1) Realizable k-ε model

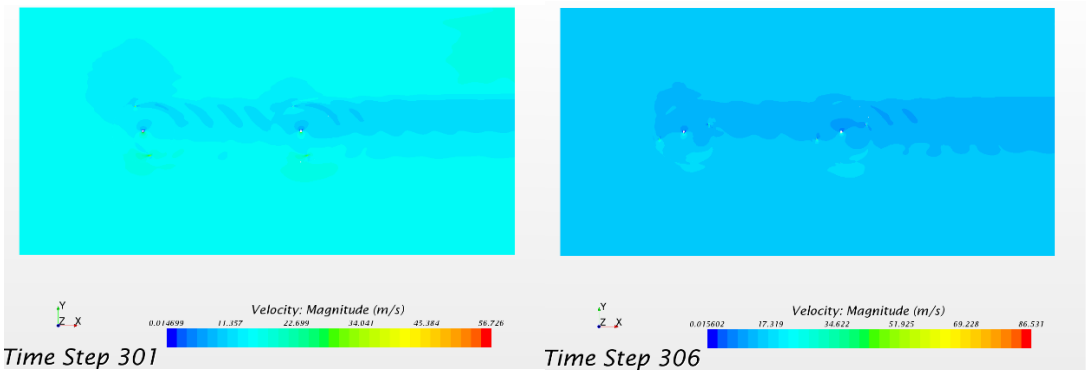

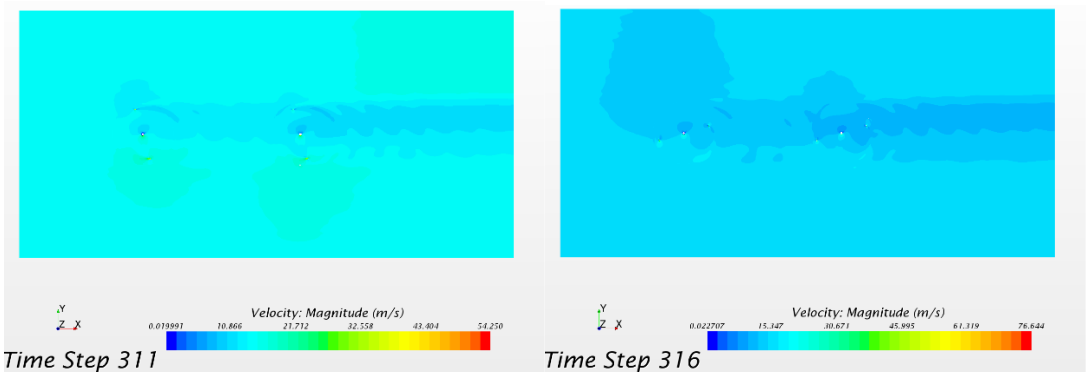

2) SST k-ω model

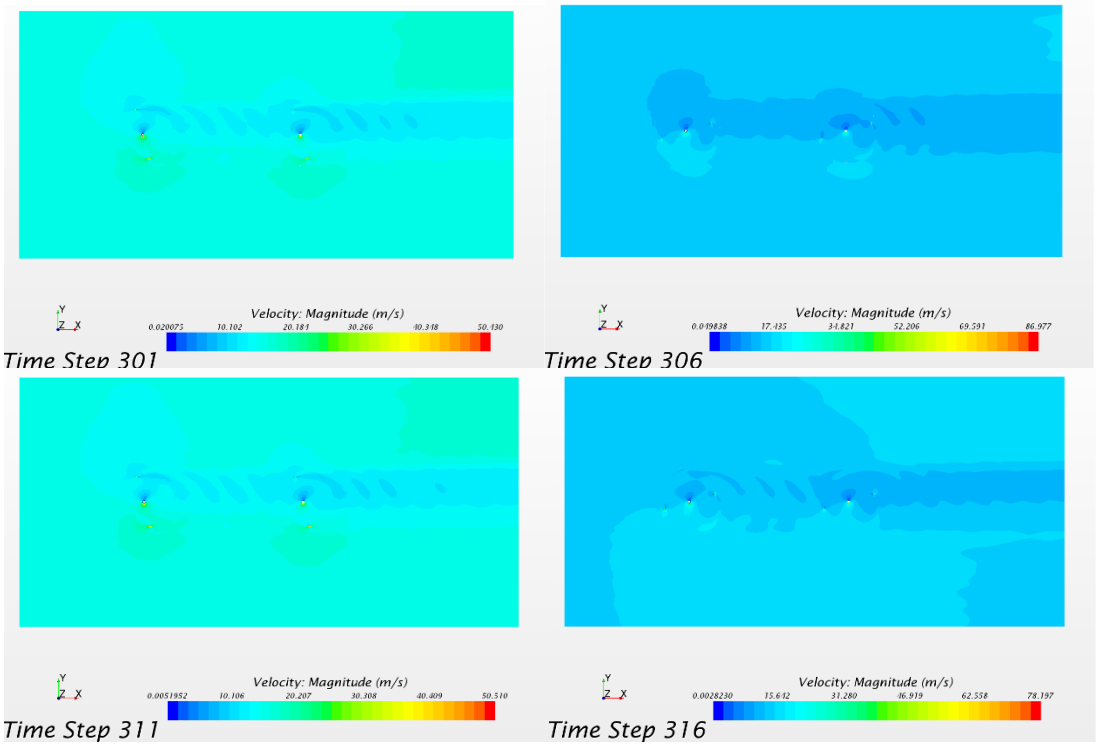

3) Sparlart-Allmaras

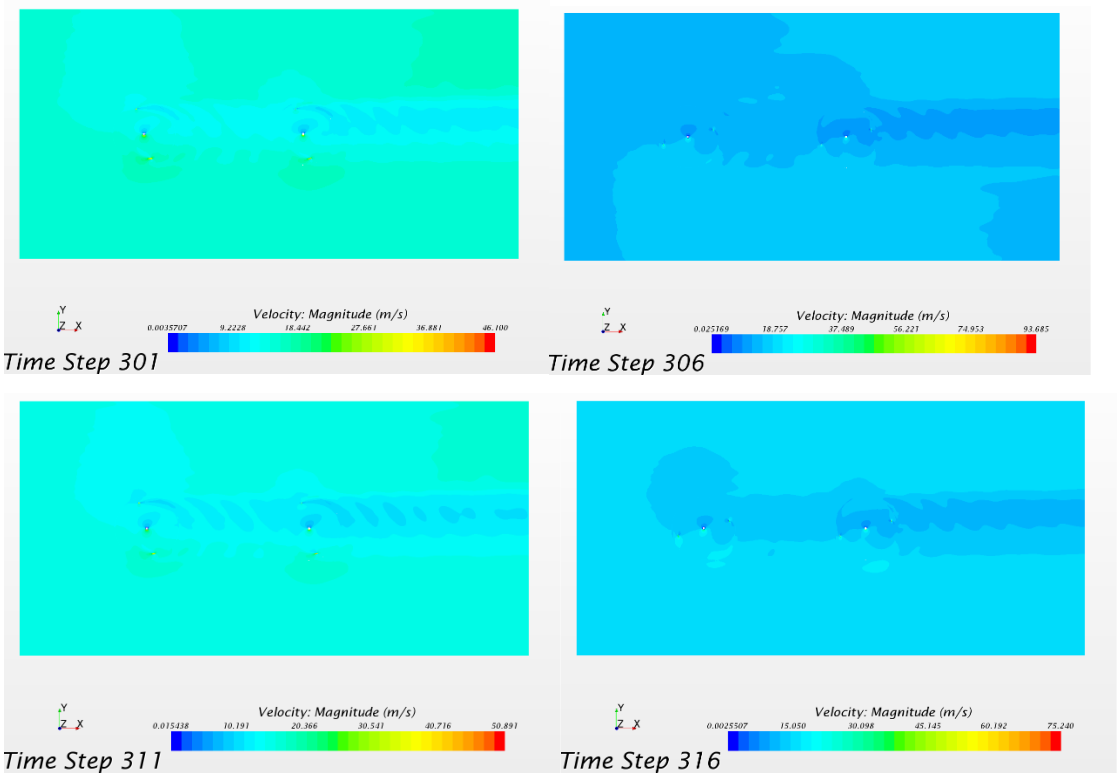

Figure 4-9 Wake velocity contour of VAWT array

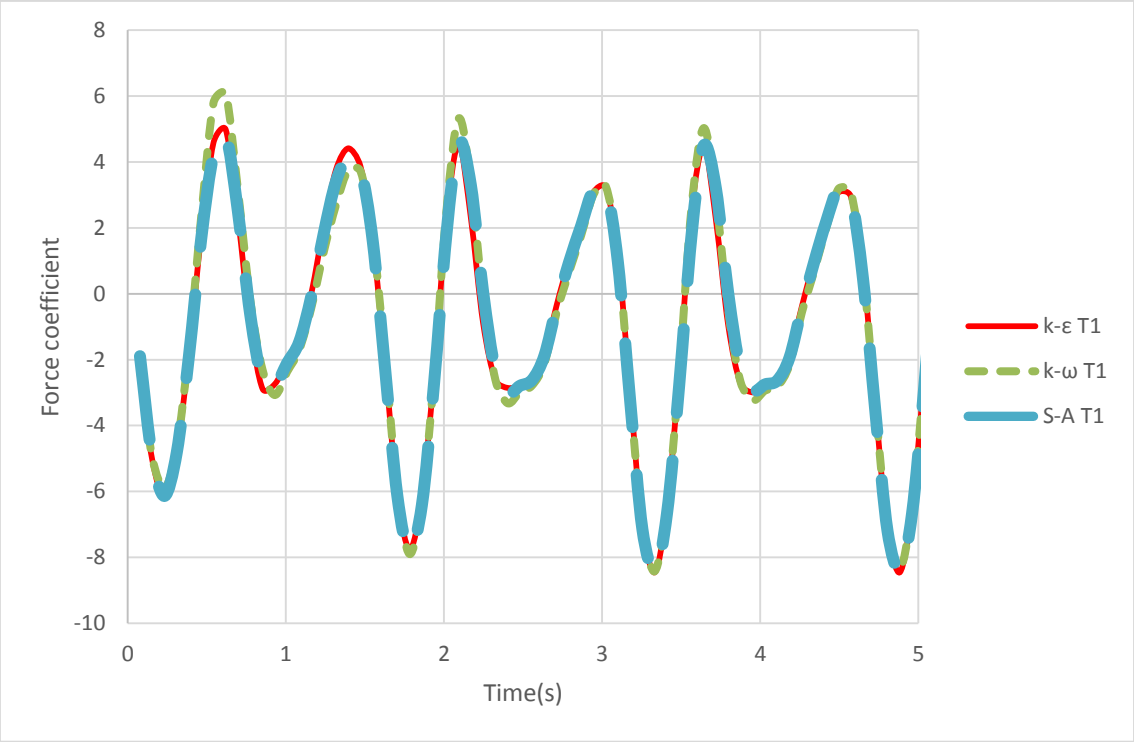

Figure 4-10 Force coefficient of upstream VAWT

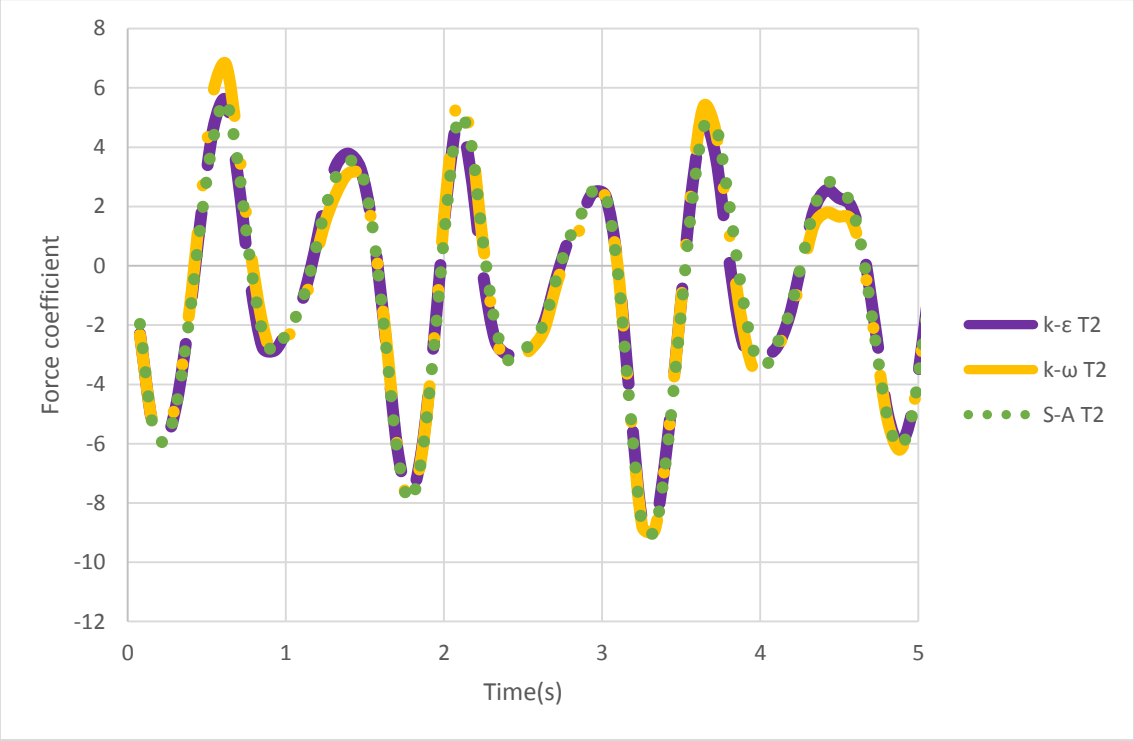

Figure 4-11 Force coefficient of downstream VAWT

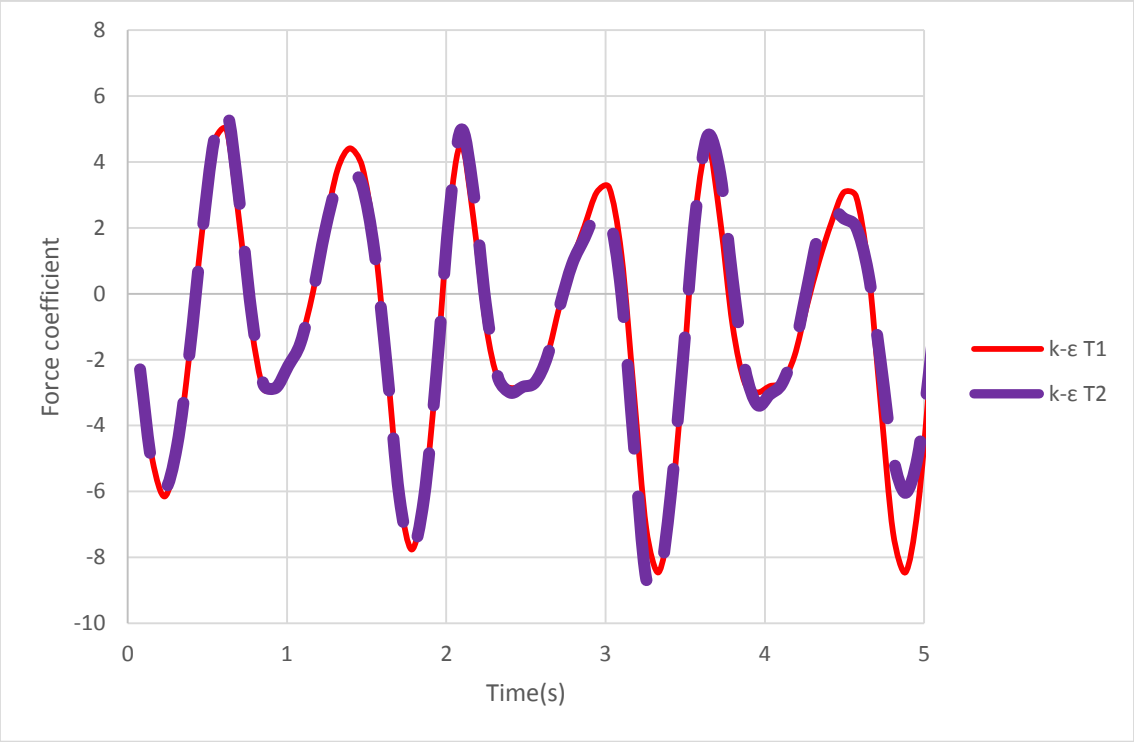

Figure 4-12 Force coefficient of two VAWTs (k-ε)

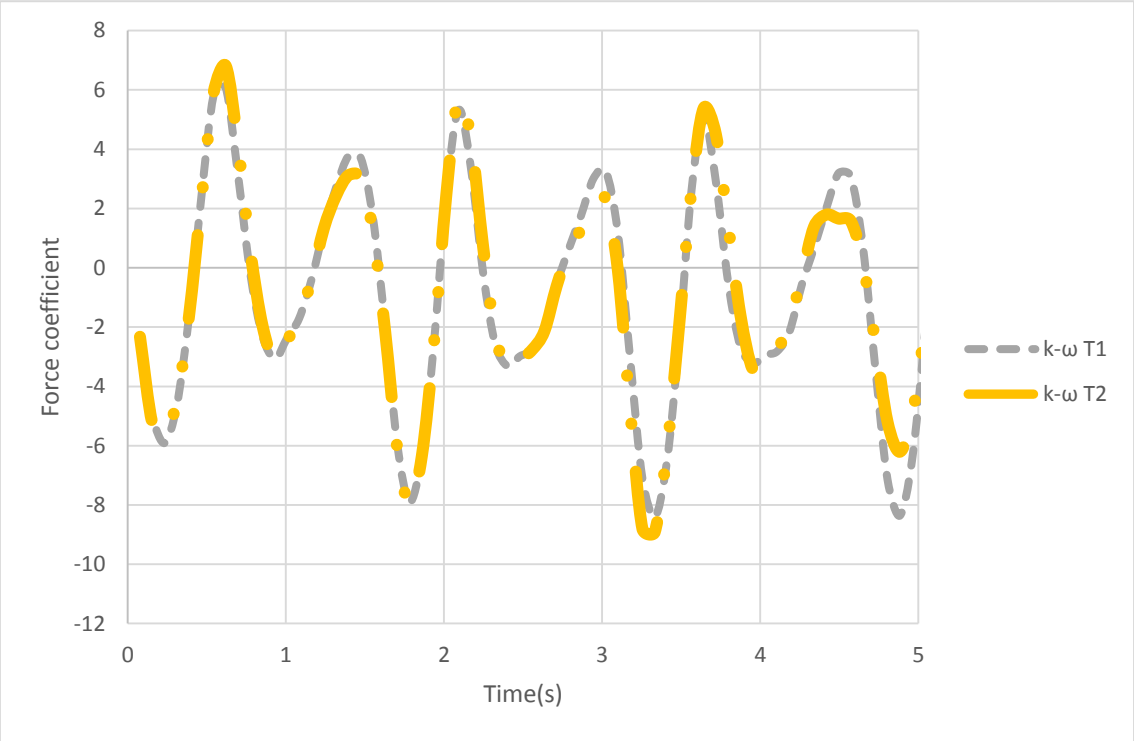

Figure 4-13 Force coefficient of two VAWTs (k-ω)

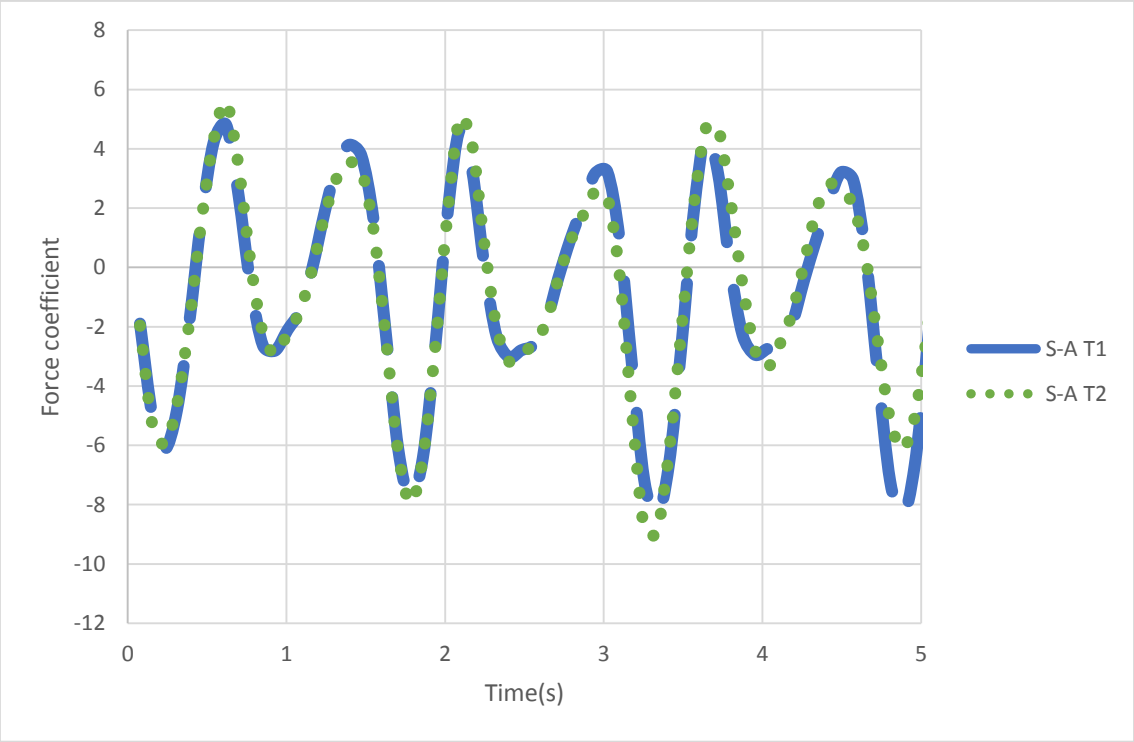

Figure 4-14 Force coefficient of two VAWTs (S-A)

4.5 Summary

In this chapter, far wake modelling of VAWT is performed on STAR-CCM+. Different approach for simulating far wake of wind turbine are presented.

Porous disk modelling was carried out to study the influence of turbulence model parameter on the far wake prediction.

The far wake modelling of a single VAWT is based on a refined mesh of the near wake modelling case in previous section, Results indicate the dependence of VAWT wake on the tip-speed ratio

Far wake modelling of two VAWT array is carried out based on polyhedral mesh. This can improve the mesh conformity in multiple region cases in modelling rotating wind turbine. An asymmetry wake profile can be observed from the VAWT array simulation., this agrees with some early experiment observation. Superposition of wake is observed. The force coefficient is altered at on the presence of this wake effect, indicating a potential structural and performance significant of wake effects to VAWT.

Different turbulence closure models are applied to the simulation, but the results indicate there is no significant difference in the three turbulence models tested.

5 CONCLUSION

5.1 Summary and Conclusion

Overall, All the research objectives are achieved for the thesis.

From the literature reviewed, it is found that the researchers have overlooked the study of VAWT wake effects. existing models are not well validated with VAWT and there is a need to understand the VAWT wake effects. CFD was applied to study HAWT wake effects and used in modelling the atmospheric turbulence.

VAWT wake effects are more difficult to simulate because of operation of VAWT, which introduces dynamic stall and flow separation at high Reynolds number. Therefore, the flow separation of cylinder at high Reynolds number and dynamics stall of a symmetry airfoil is modelled. The results indicate that the proposed RANS method can predict both phenomenon. It is also shown that the one-equation Spalart-Allmaras model yields better prediction than the two equation models in the deep stall regime. The CFD results are generally better than some indicial model.The prediction results of aerodynamic forces of a rotating VAWT under two tip speed ratios are compared with experiment data. At high tip-speed ratio the prediction is in good agreement with experiment and prediction of DMST and Vortex model. As for low tip speed ratio case, the fluctuation in the force prediction is large. The is due to the flow separation at high angle of attack. The predictions vary little over different turbulence models.

As for the far wake modelling, symmetrical wake profile is observed for the porous disk modelling case. Different methods to modify the turbulence models are applied on STARCCM+. The simulation implies that the turbulence intensities may not be as significant a factor to affect the far wake modelling.

Far wake modelling based on a full rotor configuration is performed for a single VAWT under two different tip-speed ratios, significant velocity deficits are observed for both tip speed ratios, and the for the high tip speed ratio case, the wake is much more persistent. The results indicate the dependence of VAWT wake on the wake tip-speed ratio.

Full rotor 2D modelling of VAWT array was also performed, where an asymmetry wake profile can be observed from the VAWT array simulation. The predictions agree with some early experiment observation. Superposition of wakes is significant for the both cases studied.

For two-VAWTs array where identical turbines at 3 diameters apart, the maximum force coefficients on blade is reduced by 25% at the presence of the wake effect.

5.2 Contribution to Knowledge

1 The thesis contributes to knowledge by demonstrating a comprehensive CFD study for VAWT wake effects (both near wake and far wake) on STAR-CCM+, the aerodynamic performance and wake velocity are determined.

2 The influence of different turbulence models (SST k-ω, Realizable k-ε, Sparlart Allmaras) on predicting wake effects are studied. Little difference is found across the model studied. One-equation Spalart-Allmaras model gives better predictions in capturing the deep stall phenomenon.

3 In addition, the proposed RANS method with full rotor configuration predicts an asymmetric and persistent wake region, indicating some discrepancy of wake models that assume axisymmetric wake.

5.3 Limitation and Future Work

The simulation is restricted in 2D, and 3D simulation should be considered in the future.

The results are restricted to the available turbulence models, more turbulence model should be considered in the future.

The simulation is restricted in one type of VAWT, VAWTs of different types should be considered in the future.

Ambient turbulence is not considered in the 2D simulation, effects like wind shear should be considered in the future.

The simulation is restricted in wake models and aerodynamic study, structural dynamics and structural integrity should be considered for the future.

ABBOTT, I. H. & VON DOENHOFF, A. E. 1959. *Theory of wing sections: including a summary of airfoil data*, Dover Publications.

AINSLIE, J. F. Development of an eddy-viscosity model for wind turbine wakes. Proceedings of 7th BWEA wind energy conference, 1985 1985 UK.

AINSLIE, J. F. 1988. Calculating the flowfield in the wake of wind turbines. *Journal of Wind Engineering and Industrial Aerodynamics,* 27**,** 213-224.

AKINS, R. E. 1989. Measurements of surface pressures on an operating vertical-axis wind turbine. Sandia National Labs., Albuquerque, NM (USA); Washington and Lee Univ., Lexington, VA (USA).

ALLET, A. & PARASCHIVOIU, I. 1995. Viscous Flow and Dynamic Stall Effects on Vertical-Axis Wind Turbines. *International Journal of Rotating Machinery,* 2**,** 1-14.

AMMARA, I., LECLERC, C. & MASSON, C. 2002. A viscous three-dimensional differential/actuator-disk method for the aerodynamic analysis of wind farms. *Journal of Solar Energy Engineering, Transactions of the ASME,* 124**,** 345-356.

BAGAI, A., LEISHMAN, J. G. & PARK, J. 1999. Aerodynamic analysis of a helicopter in steady maneuvering flight using a free-vortex rotor wake model. *Journal of the American Helicopter Society,* 44**,** 109-120.

BARTHELMIE, R., LARSEN, G., PRYOR, S., JØRGENSEN, H., BERGSTRÖM, H., SCHLEZ, W., RADOS, K., LANGE, B., VØLUND, P., NECKELMANN, S., MOGENSEN, S., SCHEPERS, G., HEGBERG, T., FOLKERTS, L. & MAGNUSSON, M. 2004. ENDOW (efficient development of offshore wind farms): modelling wake and boundary layer interactions. John Wiley & Sons, Ltd.

BARTHELMIE, R. J., FOLKERTS, L., LARSEN, G. C., RADOS, K., PRYOR, S. C., FRANDSEN, S. T., LANGE, B. & SCHEPERS, G. 2006. Comparison of wake model simulations with offshore wind turbine wake profiles measured by sodar. *Journal of Atmospheric and Oceanic Technology,* 23**,** 888-901.

BARTHELMIE, R. J., RATHMANN, O., FRANDSEN, S. T., HANSEN, K., POLITIS, E., PROSPATHOPOULOS, J., RADOS, K., CABEZÓN, D., SCHLEZ, W., PHILLIPS, J., NEUBERT, A., SCHEPERS, J. G. & VAN DER PIJL, S. P. 2007. Modelling and measurements of wakes in large wind farms. *Journal of Physics: Conference Series,* 75.

BERGELES, G., MICHOS, A. & ATHANASSIADIS, N. 1991. Velocity vector and turbulence in the symmetry plane of a Darrieus wind generator. *Journal of Wind Engineering and Industrial Aerodynamics,* 37**,** 87-101.

BOSSANYI, E. 2003. GH Bladed: Theory Manual.

BOSSANYI, E. A., MACLEAN, C., WHITTLE, G. E., DUNN, P. D., LIPMAN, N. H. & MUSGROVE, P. J. 1980. EFFICIENCY OF WIND TURBINE CLUSTERS. *Precision Engineering***,** 401-416.

BURTON, T., SHARPE, D., JENKINS, N. & BOSSANYI, E. 2001. *Wind Energy Handbook*, John Wiley & Sons.

CANTWELL, B. J. 1976. *A flying hot wire study of the turbulent near wake of a circular cylinder at a Reynolds number of 140,000.*

CD-ADAPCO 2014. *USER GUIDE STAR-CCM+ version 9.04*, CD-adapco™.

CRESPO, A. & HERNANDEZ, J. 1986. A numerical model of wind turbine wakes and wind farms. *IN: EWEC '86, EUROPEAN WIND ENERGY ASSOC.CONF.& EXHIB.PROC., (ROME, ITALY: OCT.7-9, 1986), W.PALZ; E.SESTO (EDS.),* 2 , Rome, Italy, A. Raguzzi Bookshop Sci. Publications, 1986, Session E, Paper E1**,** 111-115.

CRESPO, A. & HERNÁNDEZ, J. 1996. Turbulence characteristics in wind-turbine wakes. *Journal of Wind Engineering and Industrial Aerodynamics,* 61**,** 71-85.

CRESPO, A., HERNANDEZ, J., FRAGA, E. & ANDREU, C. 1988. Experimental validation of the UPM computer code to calculate wind turbine wakes and comparison with other models. *Journal of Wind Engineering and Industrial Aerodynamics,* 27**,** 77-88.

CRESPO, A., HERNÁNDEZ, J. & FRANDSEN, S. 1999. Survey of modelling methods for wind turbine wakes and wind farms. *Wind Energy,* 2**,** 1-24.

DABIRI, J. O. 2011. Potential order-of-magnitude enhancement of wind farm power density via counter-rotating vertical-axis wind turbine arrays. *Journal of Renewable and Sustainable Energy,* 3.

DEGLAIRE, P. 2010. *Analytical aerodynamic simulation tools for vertical axis wind turbines.* PhD, Uppsala Univeristy.

DIXON, K. 2008. *The near wake structure of a vertical axis wind turbine.* Master's thesis, TU Delft.

DIXON, K., FERREIRA, C. S., HOFEMANN, C., VAN BUSSEL, G. & VAN KUIK, G. A 3D unsteady panel method for vertical axis wind turbines. 2008. 1-10.

FERREIRA, C. S., VAN BUSSEL, G. & VAN KUIK, G. 2D CFD simulation of dynamic stall on a vertical axis wind turbine: verification and validation with PIV measurements. 2007.

GHARALI, K. & JOHNSON, D. A. 2012. Numerical modeling of an S809 airfoil under dynamic stall, erosion and high reduced frequencies. *Applied Energy,* 93**,** 45-52.

GOLDENBERG, J. & FEKETE, G. I. 1983. Mean flow energy content of boundary layer down-stream of vertical-axis wind-turbine simulators. *Journal of Wind Engineering and Industrial Aerodynamics,* 12**,** 1-14.

GORMONT, R. E. 1973. A Mathematical Model of Unsteady Aerodynamics and Radial Flow for Application to Helicopter Rotors. BOEING VERTOL CO PHILADELPHIA PA.

GWEC. 2015. *Global Wind Statistics 2014* [Online]. Brussels, Belgium: GWEC. Available: http://www.gwec.net/wp-content/uploads/2015/02/GWEC_GlobalWindStats2014_FINAL_10.2.2015.pdf 2015].

HAMADA, K., SMITH, T., DURRANI, N., QIN, N. & HOWELL, R. Unsteady flow simulation and dynamic stall around vertical axis wind turbine blades. 46th AIAA Aerospace Sciences Meeting and Exhibit, 2008.

HANSEN, M. O. L., SØRENSEN, J. N., VOUTSINAS, S., SØRENSEN, N. & MADSEN, H. A. 2006. State of the art in wind turbine aerodynamics and aeroelasticity. *Progress in Aerospace Sciences,* 42**,** 285-330.

HOLME, O. A contribution to the aerodynamic theory of the vertical-axis wind turbine. 1977. 4.

ISLAM, M., TING, D. S. K. & FARTAJ, A. 2008. Aerodynamic models for Darrieus-type straight-bladed vertical axis wind turbines. *Renewable and Sustainable Energy Reviews,* 12**,** 1087-1109.

JENSEN, N. O. 1983. A note on wind generator interaction. Denmark: Risø National Laboratory.

JIANG, D., COTON, F. N. & GALBRAITH, R. A. M. 1991. Fixed wake vortex model for vertical axis wind turbines including unsteady aerodynamics. *Wind Engineering,* 15**,** 348-360.

KATIC, I., HØJSTRUP, J. & JENSEN, N. O. A simple model for cluster efficiency. European Wind Energy Association Conference and Exhibition, 1986 1986 Italy. EWEA.

KECSKEMETY, K. M. & MCNAMARA, J. J. The influence of wake effects and inflow turbulence on wind turbine loads. Collection of Technical Papers - AIAA/ASME/ASCE/AHS/ASC Structures, Structural Dynamics and Materials Conference, 2010.

LARSEN, G. C. & RÉTHORÉ, P.-E. 2013. TOPFARM – A Tool for Wind Farm Optimization. *Energy Procedia,* 35**,** 317-324.

LEISHMAN, J. G. & BAGAI, A. 1998. Challenges in understanding the vortex dynamics of helicopter rotor wakes. *AIAA Journal,* 36**,** 1130-1140.

LEISHMAN, J. G. & BEDDOES, T. S. 1989. A Semi-Empirical Model for Dynamic Stall. *Journal of the American Helicopter Society,* 34**,** 3-17.

LISSAMAN, P. B. S. Energy effectiveness of arbitary arrays of wind turbines. American Institute of Aeronautics and Astronautics, Aerospace Sciences Meeting, 1979 1979 New Orleans.

LIU, H. T., BUCK, J. W., GERMAIN, A. C., HINCHEE, M. E., SOLT, T. S., LEROY, G. M. & SRNSKY, R. A. 1987. Field Investigation of a wake structure downwind of a VAWT in a wind farm array. Flow Research Company.

MCLAREN, K., TULLIS, S. & ZIADA, S. 2012. Computational fluid dynamics simulation of the aerodynamics of a high solidity, small-scale vertical axis wind turbine. *Wind Energy,* 15**,** 349-361.

MILBORROW, D. J. 1980. The performance of arrays of wind turbines. *Wind Energy Conversion Systems,* 5**,** 403-430.

MONTAVON, C., JONES, I., STAPLES, C., STRACHAN, C. & GUTIERREZ, I. Practical issues in the use of CFD for modelling wind farms. European Wind Energy Conference and Exhibition 2009, EWEC 2009, 2009. 3792-3800.

NEWMAN, B. G. 1977. The spacing of wind turbines in large arrays. *Energy Conversion,* 16**,** 169-171.

PARASCHIVOIU, I. 2002. *Wind Turbine Design: With Emphasis on Darrieus Concept*, Presses Internationales Polytechnique.

PARASCHIVOIU, I. & DELCLAUX, F. 1983. DOUBLE MULTIPLE STREAMTUBE MODEL WITH RECENT IMPROVEMENTS. *Journal of energy,* 7**,** 250-255.

PARASCHIVOIU, I. O. N. 1982. AERODYNAMIC LOADS AND PERFORMANCE OF THE DARRIEUS ROTOR. *J Energy,* V 6**,** 406-412.

POLITIS, E. S., PROSPATHOPOULOS, J., CABEZON, D., HANSEN, K. S., CHAVIAROPOULOS, P. K. & BARTHELMIE, R. J. 2012. Modeling wake effects in large wind farms in complex terrain: The problem, the methods and the issues. *Wind Energy*.

PONTA, F. L. & JACOVKIS, P. M. 2001. A vortex model for Darrieus turbine using finite element techniques. *Renewable Energy,* 24**,** 1-18.

PORTÉ-AGEL, F., WU, Y. T., LU, H. & CONZEMIUS, R. J. 2011. Large-eddy simulation of atmospheric boundary layer flow through wind turbines and wind farms. *Journal of Wind Engineering and Industrial Aerodynamics*.

QIN, N., HOWELL, R., DURRANI, N., HAMADA, K. & SMITH, T. 2011. Unsteady flow simulation and dynamic stall behaviour of vertical axis wind turbine blades. *Wind Engineering,* 35**,** 511-527.

QUARTON, D. C. & AINSLIE, J. F. 1990. Turbulence in wind turbine wakes. *Wind Engineering,* 14**,** 15-23.

RADOS, K., LARSEN, G., BARTHELMIE, R., SCHLEZ, W., LANGE, B., SCHEPERS, G., HEGBERG, T. & MAGNISSON, M. 2001. Comparison of wake models with data for offshore windfarms. *Wind Engineering,* 25**,** 271-280.

RADOS, K., MOSFILIS, S., STERGIANNIS, N., TOURLIDAKIS, A., CARALIS, G. & ZERVOS, A. CFD modeling approaches of wind turbine single and multiple wakes. European Wind Energy Conference and Exhibition 2012, EWEC 2012, 2012. 1842-1849.

RÉTHORÉ, P. E., FUGLSANG, P., LARSEN, G. C., BUHL, T., LARSEN, T. J. & MADSEN, H. A. TopFarm: Multi-fidelity optimization of offshore wind farm. Proceedings of the International Offshore and Polar Engineering Conference, 2011 2011. 516-524.

RHEE, M. J. 2002. A study of dynamic stall vortex development using two dimensional data from the AFDD oscilating wing experiment.

ROSHKO, A. 1954. On the Drag and Shedding Frequency of Two Dimensional Bluff Bodies.

SANDERSE, B. 2009. Aerodynamics of wind turbine wakes literature review. Netherland: ECN.

SCHLEZ, W., UMANA, A., BARTHELMIE, R., LARSEN, G., RADOS, K., LANGE, B., SCHEPERS, G. & HEGBERG, T. 2001. ENDOW: Improvement of wake models within offshore wind farms. *Wind Engineering,* 25**,** 281-287.

SHAMSODDIN, S. & PORTÉ-AGEL, F. 2014. Large Eddy Simulation of Vertical Axis Wind Turbine Wakes. *Energies,* 7.

SIMÃO FERREIRA, C. J. 2009. *The near wake of the VAWT: 2D and 3D views of the VAWT aerodynamics.* PhD Thesis, Technische Universiteit Delft, The Netherlands.

SIMÃO FERREIRA, C. J., BIJL, H., VAN BUSSEL, G. & VAN KUIK, G. 2007. Simulating Dynamic Stall in a 2D VAWT: Modeling strategy, verification and validation with Particle Image Velocimetry data. *Journal of Physics: Conference Series,* 75.

SNEL, H. 1998. Review of the present status of rotor aerodynamics. *Wind Energy,* 1**,** 46-69.

SONG, C. C. S. & YUAN, M. 1990. Simulation of Vortex-Shedding Flow About a Circular Cylinder at High Reynolds Numbers. *Journal of Fluids Engineering,* 112**,** 155-161.

STOVALL, T., PAWLAS, G. & MORIARTY, P. Wind farm wake simulations in OpenFOAM. 48th AIAA Aerospace Sciences Meeting Including the New Horizons Forum and Aerospace Exposition, 2010.

STRICKLAND, J. H. 1975. The Darrieus Turbine: a performance prediction model using multiple streamtubes. Sandia National Labouratory.

STRICKLAND, J. H., WEBSTER, B. T. & NGUYEN, T. 1979. A Vortex Model of the Darrieus Turbine: An Analytical and Experimental Study.

SUMNER, J., WATTERS, C. S. & MASSON, C. 2010. CFD in Wind Energy: The Virtual, Multiscale Wind Tunnel. *Energies,* 3**,** 989.

TEMPLIN, R. J. 1974a. Aerodynamic performance theory for the nrc vertical-axis wind turbine.

TEMPLIN, R. J. 1974b. An estimation of the interaction of windmills in widespread arrays. National Aeronautical Establishment.

VAFIADIS, K., STERGIANNIS, N., TOURLIDAKIS, A. & RADOS, K. G. Computational investigation of horizontal axis wind turbine wake. European Wind Energy Conference and Exhibition, EWEC 2013, 2013. 1692-1700.

VAN BUSSEL, G. J. W. 1992. The use of the asymptotic accelertion potential method for horizontal axis windturbine rotor aerodynamics. *Journal of Wind Engineering and Industrial Aerodynamics,* 39**,** 161-172.

VERMEER, L. J., SØRENSEN, J. N. & CRESPO, A. 2003. Wind turbine wake aerodynamics. *Progress in Aerospace Sciences,* 39**,** 467-510.

WHITTLESEY, R. W., LISKA, S. & DABIRI, J. O. 2010. Fish schooling as a basis for vertical axis wind turbine farm design. *Bioinspiration and Biomimetics,* 5.

WILLIAMSON, C. 1996. Vortex dynamics in the cylinder wake. *Annual Review of Fluid Mechanics,* 28**,** 477-539.

ZERVOS, A., HUBERSON, S. & HEMON, A. 1988. Three-dimensional free wake calculation of wind turbine wakes. *Journal of Wind Engineering and Industrial Aerodynamics,* 27**,** 65-76.